UNIVERSITÉ DU QUÉBEC À RIMOUSKI

SIMULATION ET VALIDATION EXPÉRIMENTALE DU TRAITEMENT THERMIQUE SUPERFICIEL AU LASER APPLIQUÉ À DES GÉOMÉTRIES COMPLEXES

Mémoire présenté

dans le cadre du programme de maîtrise en ingénierie

en vue de l'obtention du grade de maître ès sciences appliquées (M.Sc.A.)

PAR

© GUILLAUME BILLAUD

mars 2016

Composition du jury :

Éric Hudier, président du jury, Université du Québec À Rimouski

Abderazzak El Ouafi, directeur de recherche, Université du Québec À Rimouski

Nourredine Barka, codirecteur de recherche, Université du Québec À Rimouski

Souheil-Antoine Tahan, examinateur externe, École de Technologie Supérieure

Dépôt initial le 12 janvier 2016 Dépôt final le 15 mars 2016

REMERCIEMENTS

L’auteur de ce mémoire tient à remercier le professeur Abderrazak El Ouafi de l’UQAR d’avoir dirigé mon mémoire, pour tous les conseils qu’il m’a donnés notamment pour les vérifications expérimentales ainsi que pour le temps investi dans la correction de mes travaux.

Également, l’auteur souhaite remercier l’étudiant de l’UQAR, Al-Khader Borki pour sa contribution à la recherche, notamment par la fabrication du banc d’essais ayant servi à la vérification expérimentale ainsi que pour son assistance et ses conseils.

RÉSUMÉ

Le traitement thermique superficiel au laser est un procédé qui vise à améliorer la résistance des pièces mécaniques à l'usure et à la fatigue en augmentant la dureté des surfaces critiques. Se distinguant par son apport thermique bref et localisé, par sa capacité en matière de puissance surfacique et par ses cycles thermiques rapides et précis, ce procédé permet d'améliorer la résistance à l'usure et à la fatigue en durcissant les zones critiques superficielles de la pièce tout en limitant les risques de déformations indésirables. Les caractéristiques mécaniques de la zone durcie obtenue par traitement thermique au laser dépendent des propriétés physicochimiques du matériau à traiter et de plusieurs paramètres du procédé lui-même. L'exploitation adéquate des possibilités qu'offre ce procédé nécessite le développement de stratégies permettant de contrôler ces paramètres de manière à produire avec précision les caractéristiques désirées sans recourir au traditionnel long et couteux processus essai-erreur. L'objectif du projet consiste à analyser les relations de dépendance entre le profil de dureté et les paramètres du procédé dans le but d'établir des modèles simples permettant la prédiction du profil de dureté dans le cas de traitement de pièces mécaniques en acier AISI 4340 de géométries complexes. Une grande partie de ces analyses a été réalisée grâce à des simulations sur des modèles numériques 3D utilisant la méthode des éléments finis. Pour arriver à des modèles prédictifs consistants, une approche en trois phases a été adoptée. La première a consisté à développer le modèle 3D et à le valider expérimentalement pour des géométries simples. Cette phase a permis d'analyser les effets des différents paramètres sur le profil de dureté en se basant sur une expérimentation structurée combinée à des techniques éprouvées d'analyse statistique. Les résultats de cette étude ont conduit à l'identification des variables les plus pertinentes à exploiter pour la modélisation. La seconde phase a permis d'enrichir le modèle 3D et les résultats de simulation pour les combiner avec les données expérimentales dans le but d'élaborer les modèles prédictifs les plus précis possible. Deux techniques de modélisation ont été considérées à cet effet, soient la régression multiple et les réseaux de neurones. Enfin, la troisième phase a été consacrée au développement du modèle 3D pour des géométries complexes et à sa validation expérimentale. Ce modèle a été appliqué avec succès dans le cas d'un engrenage. Au cours des trois phases, les résultats obtenus se sont avérés très satisfaisants et ont montré une concordance remarquable entre les prédictions et les mesures expérimentales.

Mots clés: traitement thermique par laser, traitement thermique superficiel, simulation 3D, profile de dureté, réseau de neurones, engrenage

ABSTRACT

Laser surface hardening transformation is a superficial heating process which aims to enhance the wear and fatigue resistance by hardening the superficial critical areas of mechanical parts. This process is well-known by his capacity in terms of power flux density and recognized by his fast, local and accurate thermal cycles, while limiting the risks of undesirable distortion and deformation effects. The mechanical properties of the hardened surface depend of the physicochemical properties of the material as well as the heating system parameters. To adequately exploit the advantages presented by this heating method, it is necessary to develop a comprehensive strategy to control and adjust the process parameters in order to produce desired hardened surface characteristics without being forced to use the traditional and fastidious trial and error procedures. This study aims to analyse the relationship between the hardness profile and the process parameters in order to build a basic prediction models for hardness profile for AISI 4340 steel mechanical parts with complex geometries. The presented results in the study were achieved using finite elements method based numerical 3D models. To reach accurate and robust hardness profile predictive models, a three-step approach was adopted. The first step consists to develop and test experimentally the numerical 3D model for simple geometries. The model is used to evaluate the effects of different parameters on the hardness profile using a structured experimental design combined to confirmed statistical analysis tools. The results of this phase permitted the identification of the most relevant variables to use in the modeling stage. Then, the second step consists of enhancing and enriching the numerical model used to generate the modelling data base in order to improve the accuracy and the robustness of the predictive models. Two modeling techniques have been considered for the modelling purpose: multiple regression and neural networks. Finally, the third step consists of adapting various generated models to complex geometries. The models was successfully applied and experimentally confirmed in the case of a gear. The results obtained in each step were very satisfying and showed great concordance between predicted results and experimental measures.

Keywords: laser heat treatment, surface transformation hardening, 3D simulation, case depth, hardness profile, neural network, gears

TABLE DES MATIÈRES

LISTE DES TABLEAUX

LISTE DES FIGURES

INTRODUCTION GÉNÉRALE

De nos jours, le traitement thermique superficiel au laser est un procédé de plus en plus utilisé dans les industries automobiles et aéronautiques. Ce procédé vise à donner, au cœur et à la surface, des pièces mécaniques des caractéristiques différentes permettant d'améliorer leur résistance à l'usure et à la fatigue en durcissant les zones critiques superficielles tout en limitant les risques de déformations indésirables. Son avantage réside dans son apport thermique bref et localisé, sa capacité en termes de puissance surfacique et ses cycles thermiques rapides et précis. Les caractéristiques mécaniques de la zone durcie obtenue par traitement thermique au laser dépendent des propriétés physicochimiques du matériau à traiter et de plusieurs paramètres du procédé lui-même. Ce mémoire traite de la simulation et de la validation expérimentale du traitement thermique superficiel au laser des pièces mécaniques en acier AISI 4340 de géométries complexes telles que les engrenages. Il vise à analyser les effets des paramètres du procédé sur le profil de dureté dans le but d'élaborer des modèles prédictifs de la qualité du traitement thermique.

0.1-LE PRINCIPE DU LASER

Le laser (acronyme de l'anglais « **L**ight **A**mplification by **S**timulated **E**mission of **R**adiation ») se présente généralement sous la forme d'un dispositif qui émet un rayonnement cohérent sur le plan spatial et temporel. Le principe du laser repose sur trois phénomènes physiques décrivant l'interaction entre l'atome et la lumière. Le premier principe est celui de l'absorption : un atome peut recevoir et absorber un photon possédant une longueur d'onde bien définie. Il passe alors dans un état dit « excité ». Le deuxième principe est celui de l'émission spontanée : un atome excité peut revenir à son état initial (dit « état fondamental ») en émettant spontanément un photon de même longueur d'onde que celui qu'il avait absorbé. La direction et la phase du photon émis spontanément sont

aléatoires. Le troisième et dernier principe est celui de l'émission stimulée. Un atome excité qui reçoit un photon qui aurait permis de l'exciter s'il était dans son état fondamental peut se désexciter en émettant un photon dans la même direction et avec la même phase que le photon incident. Ce photon émis va alors s'ajouter au rayonnement et l'amplifier [1-3]. La **Figure 0.1** ci-après montre le principe d'amplification par émission stimulée.

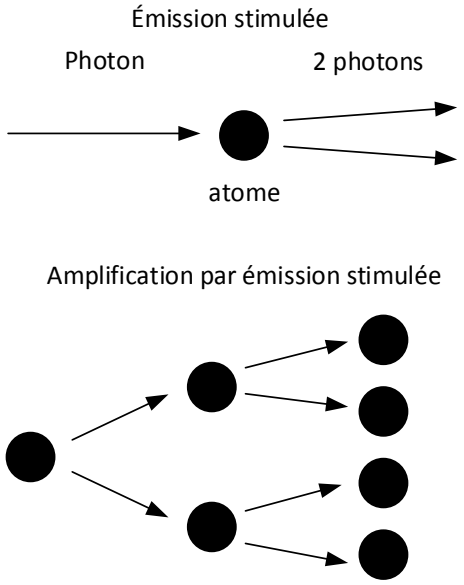

Figure 0.1 : Amplification de photons. Principe du laser

Il existe plusieurs types de laser qui se différencient par leur milieu amplificateur. Ainsi, il existe le laser à hélium néon, à argon, au krypton, au CO_2…

0.2-LE TRAITEMENT THERMIQUE DES ACIERS

L'acier est un alliage fer-carbone quelquefois combiné à d'autres éléments tels que le manganèse, le nickel, le chrome, etc. L'acier présente plusieurs phases solides (ferrite, perlite, cémentite, austénite) avec des températures de changement de phase ou d'états variables selon la teneur en carbone. La **Figure 0.2** montre les frontières entre les

différentes phases et états de l'acier. En abscisse, nous avons la teneur en carbone et en ordonnée, la température.

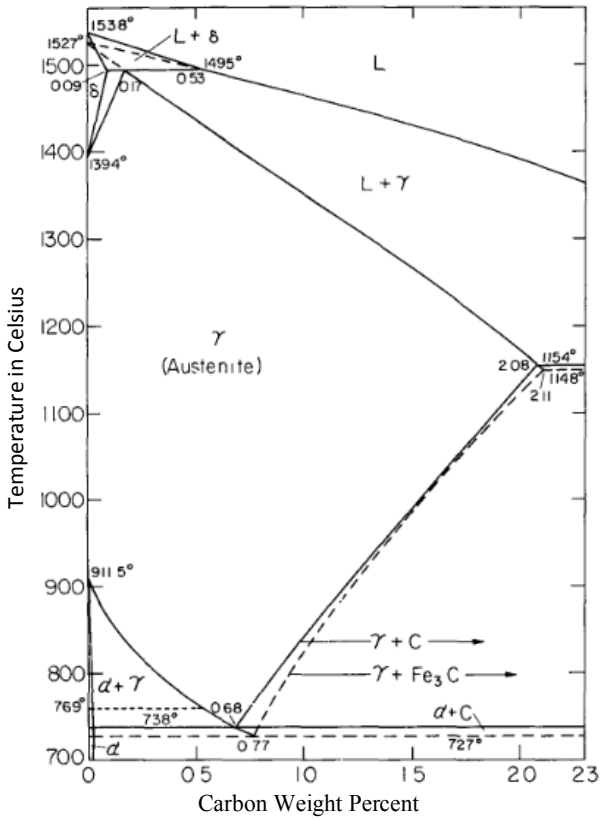

Figure 0.2 : Diagramme de phase fer-carbone [4]

Dans le cas de l'acier 4340, nous avons une teneur en carbone (C) de 0.43 % environ. Il s'agit donc d'un acier hypo-eutectoïde. La phase ferrite (α) possède une structure cristallographique cubique centrée, alors que l'austénite (γ) possède une structure cubique faces centrées. Pour réaliser le traitement thermique d'un acier, il est d'abord nécessaire de le chauffer de façon à être complètement dans le domaine austénitique. Pour l'acier 4340, une température de 1073 K suffit pour que l'acier soit complètement austénitique (voir **Figure 0.2**).

0.2.1-Le traitement thermique et ses effets

Le traitement thermique consiste à refroidir rapidement un acier à l'état austénitique. Au cours de ce refroidissement et en fonction de la vitesse de refroidissement, trois phases peuvent apparaître : la perlite, la bainite et la martensite. Ces phases ont une influence sur la dureté du matériau [5, 6]. La dureté d'un matériau se définit comme sa capacité à s'opposer à la propagation d'une dislocation (défaut linéaire qui traduit une discontinuité dans l'organisation de structure cristalline.). Le principe de traitement thermique de l'acier repose sur la diffusion des atomes de carbone et le temps de diffusion accordé à ces atomes. En effet, dans un acier austénitique, les atomes de carbone se logent dans les sites interstitiels de la structure cubique à faces centrées de l'austénite. Lors du refroidissement, ces atomes migrent vers les joints de grains s'ils en ont le temps. En dehors de la ferrite et cémentite (Fe_3C) pro-eutectoïde qui peuvent se former lors du refroidissement du matériau, trois phases influencent principalement la dureté d'un acier : la perlite, la bainite et la martensite.

0.2.1.1-La perlite

Il s'agit de la phase stable composée de lamelles de ferrite et de cémentite superposées. Ces lamelles peuvent être observées sur la **Figure 0.3**. On obtient de la perlite par un refroidissement lent de l'acier austénitique.

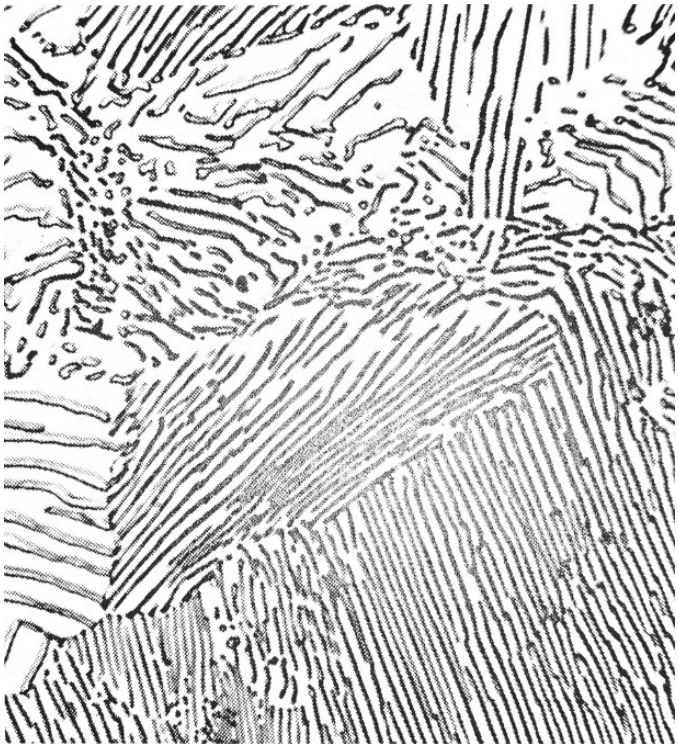

Figure 0.3 : Perlite observée au microscope 1000x [7]

La perlite peut être plus ou moins fine selon la vitesse de refroidissement. Plus le refroidissement est rapide et moins les atomes de carbone ont le temps de se diffuser vers les joints de grains et donc plus les lamelles de cémentite et ferrite sont fines. Une perlite fine est plus dure qu'une perlite grossière. En effet, le nombre d'interfaces cémentite-ferrite par unité de volume étant plus grand, les dislocations progressent plus difficilement, chaque interface étant un obstacle à son avancée.

0.2.1.2-La bainite

Cette phase présente les mêmes constituants que la perlite (ferrite et cémentite), mais possède une structure beaucoup plus fine sous forme d'aiguilles. La structure de la bainite peut être observée sur la **Figure 0.4**. On obtient de la bainite lors d'un refroidissement trop rapide pour former de la perlite (trop faible diffusion des atomes de carbone), mais pas suffisamment pour obtenir de la martensite. La bainite est plus dure que la perlite.

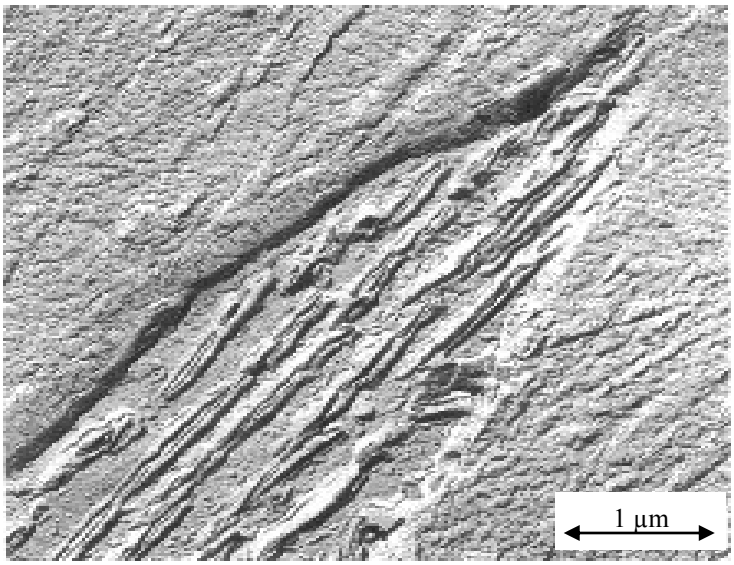

Figure 0.4 : Bainite observée au microscope

0.2.1.3-La martensite

La martensite est une phase métastable de l'acier qui s'obtient par un refroidissement très rapide de l'acier. Les atomes de carbone qui s'étaient logés dans les sites interstitiels de la structure cubique à faces centrées de l'acier austénitique n'ont pas le temps de se diffuser. Or, les sites interstitiels de la structure cubique centrée de la ferrite sont beaucoup plus petits. Les atomes de carbones se retrouvent ainsi piégés dans des espaces trop petits pour eux. Ils exercent alors des contraintes sur l'ensemble de la maille et la déforment. La déformation de la maille engendre un grand nombre d'obstacles à la propagation d'une dislocation. Cela explique la grande dureté observée dans le cas de la structure martensitique. La microstructure de la martensite peut être observée sur la **Figure 0.5**.

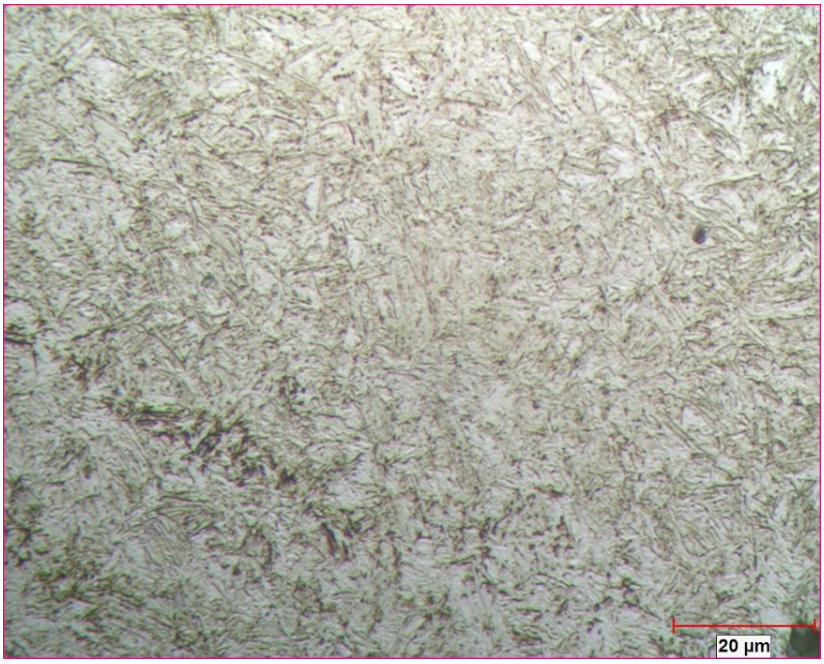

Figure 0.5 : Structure martensitique

0.3- LE TRAITEMENT THERMIQUE AU LASER

Ce traitement consiste à envoyer un rayonnement lumineux énergétique sur une zone très localisée de la pièce. Il s'en suit d'un échauffement très localisé (et très rapide) de la pièce sur une certaine profondeur. Une fois que le faisceau laser a quitté la zone frappée, le volume réchauffé (souvent très petit) se refroidit très rapidement par diffusion de la chaleur dans le reste du matériau. Dans le cas d'un traitement de surface d'un acier, le faisceau laser transmet une importante quantité d'énergie dans un petit volume de matière sous la surface. Ce volume de matière passe alors très rapidement au-dessus de la température d'austénitisation de l'acier. Puis, ce volume, en se refroidissant très rapidement, engendre l'apparition d'une structure martensitique particulièrement fine même pour des matériaux difficiles à traiter thermiquement par des méthodes conventionnelles [2]. Le principe du traitement laser est illustré sur la **Figure 0.6**. :

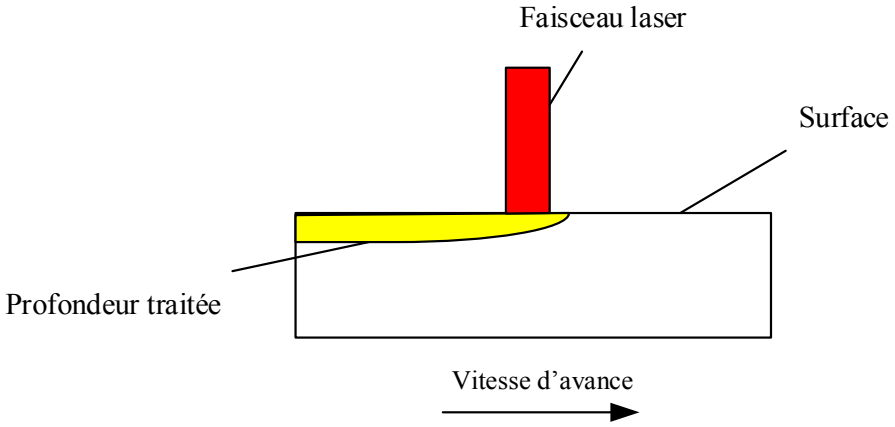

Figure 0.6 : Principe du traitement surfacique par laser

L'un des grands avantages de ce traitement est qu'il ne génère que très peu de distorsions ou de contraintes internes [1, 2]. Deux critères influencent l'efficacité du traitement de surface par laser. Pour les aciers, la zone à durcir doit être chauffée bien au-dessus de la température d'austénitisation et maintenue suffisamment longtemps au-dessus de celle-ci pour donner le temps nécessaire à la diffusion du carbone. De plus, les régions en contact direct avec la région à durcir doivent être suffisamment importantes en volume pour permettre le traitement thermique par diffusion de la chaleur vers ces régions.

Les paramètres clés du procédé sont [2] :

— La puissance de la source laser, la vitesse de balayage du laser et éventuellement les caractéristiques du gaz protégeant la pièce de l'oxydation (argon ou hélium).

— Le modèle de distribution d'énergie (gaussienne, uniforme…).

— L'absorptivité du matériau pour la longueur d'onde du laser utilisé.

— Les propriétés thermiques du matériau (chaleur spécifique, conductivité thermique) et la microstructure initiale.

Diminuer la vitesse de balayage conduit à une plus grande profondeur de traitement, mais diminue la dureté de la surface. En effet, une plus faible vitesse de balayage signifie une plus grande élévation de la température au niveau de la surface et donc un temps plus important d'austénitisation. Ce temps plus important conduit à la formation de grains d'austénite de grandes tailles et donc d'une microstructure plus grossière qui aura des répercussions, après refroidissement, sur la microstructure de la martensite et sa dureté.

La **Figure 0.7** montre, pour des vitesses de balayage différentes, un profil de dureté pour un acier AISI 4340 revenu à 649 °C pendant 2 heures et chauffé avec un laser CO_2 d'une puissance de 1.8 kW.

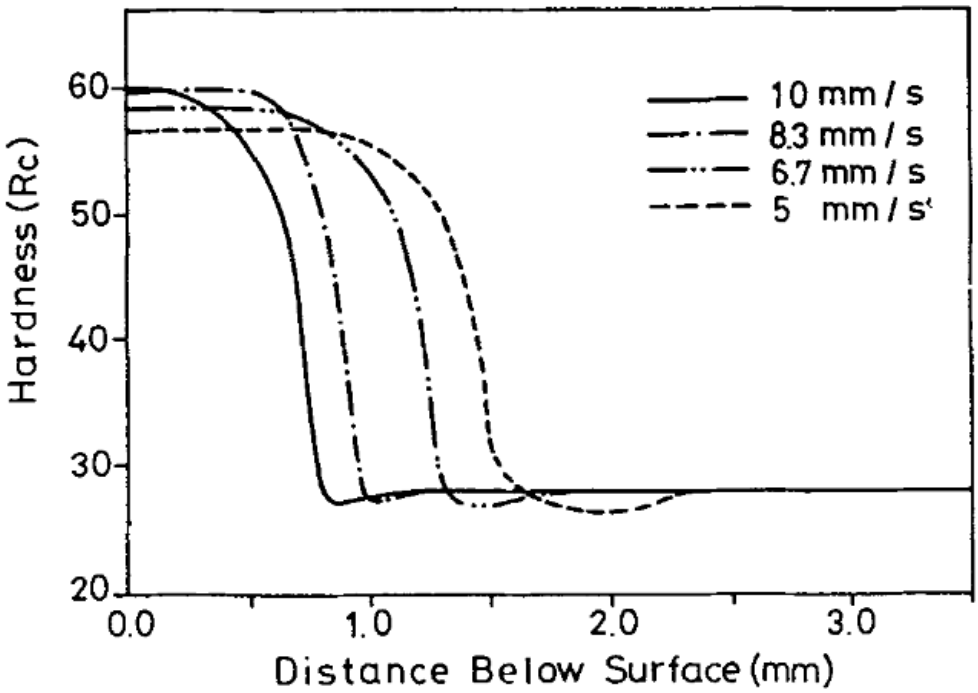

Figure 0.7 : Profils de dureté pour différentes vitesses de balayage dans le cas d'un acier AISI 4340 [8]

Sur le schéma, on remarque, pour certaines vitesses de balayage, une zone ou la dureté est inférieure à la dureté initiale du matériau. Cette zone correspond à une région non traitée, mais affectée néanmoins par la diffusion de chaleur importante dans cette région

lors du refroidissement. Cela n'est en général pas désirable et il existe des moyens pour limiter cet inconvénient.

Le mode de distribution d'énergie gaussienne (qui est admis comme étant le mode de distribution naturelle de l'énergie laser) n'est pas toujours adapté lorsqu'il est question d'un traitement de surface. En effet, la distribution non uniforme sur la tâche focale de l'énergie peut causer la fonte localisée du matériau. Pour obtenir une distribution plus uniforme de l'énergie sur une surface plus grande, on applique des méthodes de changement de forme du rayon laser grâce à des lentilles qui permettent, notamment, de dé focaliser le rayon.

L'absorptivité du matériau joue également un rôle fondamental. Elle dépend notamment de :

— la longueur d'onde de la source laser.

— L'angle d'incidence du rayon laser.

— Les propriétés thermiques du matériau et de sa microstructure.

— L'état de surface de la pièce (brute de fonderie, usinée, polie, meulée…) qui va jouer sur le coefficient de réflexion de la surface.

Pour améliorer l'absorptivité d'un matériau, plusieurs solutions sont possibles. On peut par exemple utiliser un très fin revêtement absorbant qui doit pouvoir s'adhérer à la surface, ne pas agir chimiquement avec le matériau même chauffé et être retiré facilement après le traitement.

0.4- AVANTAGES ET INCONVÉNIENTS DU PROCÉDÉ DE TRAITEMENT THERMIQUE SURFACIQUE AU LASER.

Il existe de nombreuses façons de traiter thermiquement la surface d'un acier. Les méthodes les plus courantes, autres que le laser, utilisent l'induction, le chalumeau, l'arc électrique et le faisceau d'électrons. Le **Tableau 0.1** ci-après montre les avantages et les inconvénients de chacun des procédés [3]

Tableau 0.1 : Comparaison entre les différents procédés

	Avantages	Inconvénients
Laser	-Distorsions thermiques minimales -Durcissement sélectif -aucun refroidissant requis -Possibilité de traiter les faibles épaisseurs -Profondeur de traitement contrôlable -aucun post-traitement requis -améliore la résistance en fatigue	-Équipements très onéreux -Surfaces durcies limitées lors d'une passe -revêtements thermique souvent requis -de multiples passes provoquent une fusion locale en surface.
Induction	-Production rapide -Possibilité d'avoir de faibles profondeurs traitées -les coûts ont plus faibles que pour le laser -Surfaces de traitement importantes.	-Temps de pause obligatoire pour changer les spires -Distorsions thermiques -faible flexibilité due à l'importance de la place, de la forme et de la taille des spires -Fortes pénétrations thermales -Dégradation possible de l'état de surface
Chalumeau	-Peu onéreux -flexible -transportable	-Mauvaise reproductibilité -Traitement thermique relativement lent -forte probabilité de distorsions thermiques des pièces -Problèmes environnementaux
Arc électrique	Relativement peu onéreux et flexible	-Épaisseur de section limitée -larges pénétrations thermales Fusion de l'acier difficilement contrôlable

Faisceau d'électrons	-Distorsions thermiques minimales - Traitement sélectif - Aucun refroidissant requis	-Équipements très onéreux -faire le vide est requis -faible productivité -Coût important d'opération

0.5-PROBLÉMATIQUE GÉNÉRALE

Le procédé de traitement thermique au laser est de plus en plus employé dans l'industrie automobile et aéronautique. Les composantes ainsi traitées telles que les engrenages se distinguent par de meilleures performances comparativement à celles produites par des procédés conventionnels [9]. Du point de vue industriel, le procédé présente plusieurs avantages comparativement aux procédés de traitement thermochimiques. Premièrement, le temps de traitement est très court et ne dépasse pas quelques secondes. Deuxièmement, le traitement ne provoque pas de distorsions thermiques majeures des composantes mécaniques développées du fait que la pièce est superficiellement chauffée. Troisièmement, le procédé peut être facilement intégré dans des cellules de fabrication. Finalement, le procédé ne fait usage d'aucun gaz et reste très flexible comparé à la méthode de traitement par induction [1, 10].

Malgré les avantages du procédé, il reste difficile à intégrer à grande échelle dans les chaînes de production. En effet, les compagnies manufacturières ont besoin d'atteindre de grandes performances et d'avoir des recettes de développement fiables et peu couteuses avant d'adopter un procédé. En effet, l'état actuel des connaissances et du savoir-faire oblige les industriels à chercher les paramètres optimaux en se basant sur les méthodes par essais et erreurs. Ces procédés industriels sont très couteux et demandent un grand temps de développement. De plus, ils ne permettent pas d'obtenir une meilleure compréhension du comportement global du procédé et de bien cerner tous les phénomènes en jeu [1]. En effet, l'aspect multiphysique du procédé et les interactions entre le faisceau laser et le transfert de chaleur affectent grandement le comportement du procédé [2]. De plus, plusieurs variables telles que les paramètres du procédé et les propriétés du matériau affectent le comportement

global du procédé. Les propriétés du matériau varient en fonction de la température et de la vitesse de chauffe. De plus, ces propriétés ne sont pas connues dans les conditions hors équilibre thermodynamique. La complexité des interactions entre les phénomènes thermiques, métallurgiques et mécaniques rend difficile l'établissement de modèles fiables capables de prédire le profil de dureté en fonction des paramètres du procédé.

L'exploration systématique du procédé n'a jamais eu lieu en utilisant une approche claire combinant l'étude des propriétés du matériau et des paramètres du procédé dans des conditions hors équilibre thermodynamique [3]. Dans ce sens, la simulation par éléments finis constitue un outil puissant pour mieux comprendre le comportement global du procédé de traitement thermique au laser et pour quantifier l'effet des paramètres de simulation sur la distribution de la température. Les modèles à développer doivent être basés sur les méthodes numériques par éléments finis afin de résoudre les équations gouvernant le champ thermique (Fourrier-Kirchhoff). La revue de littérature menée dans le cadre de ce projet de recherche indique clairement que les recherches effectuées ont permis d'approcher correctement le procédé de traitement thermique au laser, mais sans mettre en place des approches capables de dégager concrètement les effets réels des propriétés du matériau ou des paramètres du procédé sur le profil de dureté [4].

0.6-OBJECTIF

Le projet vise à étudier et surtout à prédire le profil de dureté en surface de pièces mécaniques en acier, à géométries simples ou complexes, traitées thermiquement au laser. Dans cette optique, il sera question de l'élaboration de modèles numériques 3D du procédé en utilisant les éléments finis. Les résultats générés par ces modèles numériques seront comparés aux essais expérimentaux.

0.7-MÉTHODOLOGIE

Dans un premier temps, il s'agit de pouvoir simuler avec un logiciel capable d'effectuer un calcul par éléments finis le procédé de transformation surfacique au laser dans le cas d'une géométrie simple. Le but de cette première étape est d'avoir une idée de la nature des différents phénomènes physiques qui entrent en jeu dans ce procédé ainsi que de leurs effets sur la microstructure de l'acier. Ensuite, le modèle doit aussi pouvoir générer rapidement des résultats utilisables dans des études complémentaires afin d'avoir un quelconque intérêt économique. Le modèle numérique doit bien sûr être robuste, c'est-à-dire adaptable à n'importe quelle géométrie et avec n'importe quel ensemble de paramètres de contrôle. Enfin, et surtout, les résultats donnés par le modèle numérique doivent être vérifiés par des essais expérimentaux dans plusieurs cas de figure avec des paramètres de contrôle différents.

Une fois un modèle numérique établi et vérifié dans le cas d'une géométrie simple, il sera adapté aux géométries complexes que sont les engrenages. Les résultats dans le cas d'une géométrie complexe devront aussi être vérifiés par des essais expérimentaux.

0.8-ORGANISATION DU MÉMOIRE

Le présent mémoire se divise en trois chapitres. Le premier chapitre se concentre sur l'établissement d'un modèle de simulation en trois dimensions du procédé de traitement thermique superficiel au laser dans le cas d'une géométrie simple. Un simple balayage de la pièce dans le sens de sa longueur est alors réalisé avec une sélection spécifique de paramètres (puissance, vitesse de balayage et diamètre du focus) différents à chaque simulation. L'historique des températures est alors extrait du logiciel et utilisé pour déterminer le profil de dureté grâce aux équations métallurgiques de Ashby et Easterling [5]. Ensuite, ces profils de dureté simulés sont comparés aux profils de dureté réels observés provenant de tirs au laser avec les mêmes ensembles de paramètres. De façon générale, ce premier chapitre permet mieux comprendre les phénomènes thermiques qui

entrent en jeu dans le procédé de traitement thermique au laser et d'établir une bibliographie sur l'ensemble des recherches effectuées sur le sujet.

Le deuxième chapitre reprend la géométrie simple traitée dans le premier chapitre, mais utilise une autre modélisation : le laser est modélisé comme un flux de chaleur au lieu d'une source de chaleur comme dans le premier chapitre. Cette modélisation à l'avantage d'être plus facile à implémenter surtout en prévision d'un passage aux géométries complexes. Le chapitre traite également de l'utilisation ultérieure des données de simulation afin de réaliser des études statistiques précises ainsi que l'entrainement d'un réseau de neurones. Le réseau de neurones, une fois entrainé grâce aux données de simulation, est capable de donner les caractéristiques du traitement thermique selon les paramètres d'entrée, et cela, indépendamment du logiciel de simulation.

Le troisième chapitre aborde les géométries complexes (plus particulièrement les engrenages) et reprend la modélisation en flux de chaleur du deuxième chapitre. En outre, dans ce chapitre, un mouvement de rotation de l'engrenage vient s'ajouter au mouvement de translation du faisceau laser. Un banc d'essai incluant un tour en rotation a été spécialement conçu et installé dans la cellule laser de l'UQAR pour le traitement thermique des engrenages. Le procédé en lui-même contient une phase indispensable de préchauffage puis une phase de traitement. Ce banc d'essai a permis la validation des résultats obtenus lors de la simulation. Les résultats obtenus par le procédé sont assez comparables avec ceux obtenus par le traitement par induction qui reste le procédé le plus utilisé aujourd'hui dans l'industrie. Cependant, le procédé développé dans cette étude à l'avantage d'être robuste. En effet, un seul montage permet le traitement d'engrenages de diamètres différents ce qui n'est pas le cas avec le traitement par induction.

CHAPITRE 1
PRÉDICTION DU PROFIL DE DURETÉ D'UNE PLAQUE EN ACIER 4340 TRAITÉE THERMIQUEMENT AU LASER EN UTILISANT UN MODEL 3D ET UNE VALIDATION EXPÉRIMENTALE

1.1-RESUME EN FRANÇAIS DU PREMIER ARTICLE

L'article présente l'étude du traitement thermique au laser d'une plaque en acier 4340 au moyen d'un logiciel commercial de simulation. Le but de l'étude est d'être capable de prédire quel sera le profil de dureté en fonction des paramètres de contrôle du procédé tels que la puissance, la vitesse de balayage et le diamètre du faisceau) et cela, sans nécessiter une étude expérimentale onéreuse. Ainsi, il sera possible d'obtenir la dureté en surface désirée au premier essai et donc de faire des économies. La première partie de l'article se concentre sur la mise en place du modèle 3D et de l'intégration dans le logiciel des équations thermiques et métallurgiques. La deuxième partie concerne la génération de différents profils de dureté avec différentes combinaisons de paramètres de contrôle. L'effet de chacun des trois paramètres de contrôle sur le profil de dureté est alors analysé. Enfin, dans la troisième partie, nous validons expérimentalement les résultats de simulation en comparant, deux à deux, les profils de dureté réels et simulés pour différentes combinaisons de paramètres. L'étude montre que les combinaisons de paramètres (puissance, vitesse de balayage) doivent être choisies judicieusement pour permettre le traitement de l'acier sans atteindre le point de fusion en surface. Globalement, les résultats obtenus sont satisfaisants avec de faibles écarts entre profils simulés et profils réels.

Ce premier article, intitulé « *Prediction of hardness profile of 4340 steel plate heat treated by laser using 3D model and experimental validation* », fut corédigé par moi-même ainsi que par les professeurs Noureddine Barka et Abderrazak El Ouafi. Il fut accepté pour publication dans sa version définitive en 2014 par l'American Society of Mechanical Engineers (ASME). En tant que premier auteur, ma contribution à ce travail fut l'essentiel de la recherche sur l'état de l'art, le développement de la méthode, l'exécution des tests de performance et la rédaction de l'article. Les professeurs Noureddine Barka et Abderrazak El Ouafi, respectivement second et troisième auteur, ont fourni l'idée originale. Ils ont aidé à la recherche sur l'état de l'art, au développement de la méthode ainsi qu'à la révision de l'article. Ahmed Chebak et Jean Brousseau ont contribué à la révision de l'article. Une version abrégée de cet article a été présentée, sous forme d'affiche, à la conférence *International Mechanical Engineering Congress & Exposition (IMECE)* à Montréal à l'automne 2014.

1.2-PREDICTION OF HARDNESS PROFILE OF 4340 STEEL PLATE HEAT TREATED BY LASER USING 3D MODEL AND EXPERIMENTAL VALIDATION

G. Billaud
Mathematics, Computer and Engineering Department
University of Quebec at Rimouski
Rimouski, Canada, G5L 3A1

N. Barka
Mathematics, Computer and Engineering Department
University of Quebec at Rimouski
Rimouski, Canada, G5L 3A1

A. El Ouafi
Mathematics, Computer and Engineering Department
University of Quebec at Rimouski
Rimouski, Canada, G5L 3A1

A. Chebak
Mathematics, Computer and Engineering Department
University of Quebec at Rimouski
Rimouski, Canada, G5L 3A1

J. Brousseau
Mathematics, Computer and Engineering Department
University of Quebec at Rimouski
Rimouski, Canada, G5L 3A1

1.2.1-abstract

This paper presents a study of hardness profile of 4340 steel plate heat treated by scanning laser technique using 3D model. The proposed approach is carried out in three distinguished steps. First, a 3D model is developed using an adequate formulation and taking into account the nonlinear behaviour of the material. Then, the hardness curve is approximated from the temperature distribution using metallurgical assumptions related to the kinetic transformation and the temperature-time transformation diagram. Then, the case depth is quantitatively analyzed versus the beam power density and scanning speed. Finally, the developed approach is validated using experimental tests. The gap between simulation and experimental results is determined. The obtained results allow predicting of the hardness profile with a fairly good accuracy.

1.2.2-Nomenclature

Ac_1 Eutectoid temperature (K)

Ac_3 Austenitization temperature (K)

Ac Steel absorption coefficient (m-1)

c Carbon content of steel (wt %)

c_c Critical value of carbon composition

c_e Eutectoïde carbon composition (0.8% C)

c_f Carbon in ferrite (0.01% C)

Cp Specific heat (J/kg.K)

D_0 Pre-exponential of diffusion of carbon (m2/s)

f Volume fraction of martensite

fm Maximum volume fraction of martensite

fi Volume fraction occupied by the pearlite colonies

g Average grain size (µm)

Hm Hardness of the martensite (HV)

K Thermal conductivity (W/m.K)

Lz Plate thickness

P Laser power (W)

Q Activation energy of diffusion of carbon (J/mol)

R Gas constant (J/mol.K)

Rc Reflection coefficient

t Time (s)

$T(t)$ Heat cycle temperature (K)

T_0 Reference temperature (K)

V_0 Laser translational velocity (mm/s)

w Gaussian beam radius (mm)

ρ Density (kg/m3)

1.2.3-Introduction

Nowadays, laser surface hardening is becoming more and more used in aerospace and automotive industries. This is due to the selected and local heat treatment character and

the high performances of mechanical component that it is capable of providing. Moreover, the process provides hard surface layers with low levels of distortion in a very short time [2, 3]. In fact, the distortions are less important than those obtained by flame, induction heating and thermochemical hardening processes such as carbonizing and nitriding [11]. In addition, the process offers the possibility to be fairly and precisely numerically controlled. When the power density is applied and the scanning speed is adjusted, the laser beam induces thermal flux within the part surface. Consequently, the initial microstructure is transformed completely into austenite after reaching the austenitizing temperature (Ac_3). Then, it becomes martensite upon its self-quenching through heat conduction into the colder bulk of the part core [12]. However, the heating stage must be long enough for the carbon to be diffused and the austenitization to be completed. The quenching stage must be fast enough to create fine martensite and to prevent the natural austenite degradation into perlite or bainite [13]. Conversely, due to temperature gradients, it happens that below the surface, as the depth increases, local and different austenitizing and quenching conditions appears. This leads to dissimilar degrees of austenite homogenisation and thus, dissimilar degrees of martensite homogenisation [14].

Despite the industrial advantages exhibited by the laser heat treatment process, it still remains difficult to predict with a good accuracy the hardness profile based on the process setting. Indeed, the process is affected by parameters such as input power, beam size and scanning speed as well as the nonlinear properties of the material such as thermo-physical and metallurgical properties [2, 3]. It is true that numerical simulation models combining heat conduction modes and metallurgical transformations can be advantageous to understand the qualitative and quantitative influences of each parameter on the process. However, they are not accurate enough and reality representative to predict results such as hardness profiles, case depths and compressive residual stresses with a good accuracy.

Since the heat treatment process consists of a fast laser heating, it is difficult to characterize all physical quantities such that the generated heat amount and the temperature distribution during surface transformation. The process is so fast that the measurement devices such as the thermocouples or pyrometers are not able to follow the process

dynamic due to the time constant. The interference effects affect the quality of measured signal playback. In addition, the calibration of this instrument is performed under specific conditions and depends greatly on the material emissivity.

Literature review conducted during this work allows synthetizing the development efforts done in the laser heat treatment field. Many studies propose some numerical models based on thermal and metallurgical equations in order to establish a relationship between the case depth and the process parameters variation [15]. The hardness profile is closely depending on the temperature distribution and the metallurgical transformations occurred during heating. These models could be exploited in order to predict hardness profile under some specific conditions. The thermal model usually resolves the transient heat based on heat-flow equation to find the temperature distribution [2, 16]. Generally, the Finite Element Method (FEM) is used to solve the equation with time dependant parameters [15-17]. There is an interesting exception where a Finite Difference Method (FDM) is used to solve the thermal equation which is less time consuming but also less accurate [18]. Once the temperature distribution is determined, metallurgical equations allow predicting the phase transformation and thus the hardness profile. In this way, the Johnson-Mehl-Avrami and Koistinen-Marburger equations are used to predict the phase transformation which are based on the discretization of the Time-Temperature-Transformation (TTT) diagram [16]. Moreover, equations from Ashby and Easterling are used as the metallurgical model to determine the phase transformation [19, 20]. Once the phases' proportions are computed, the Maynier equations are usually used to calculate the final hardness profile using a mixture rule [21]. Note that the result of those simulations usually do not show the over tempered zone, where the hardness becomes inferior to the initial hardness of material, which can be highlighted by the experimental study under certain initial microstructural properties [8]. Finally, there is no based-simulation study for the laser surface hardening process of the AISI 4340 steel and the studies usually do not compare the effectiveness of the process with other hardening process like induction, nitriding, etc.

This paper aims to predict the hardness profile of plate made in 4340 steel and hardened by laser process as a function of the beam power and the scanning speed. The

proposed 3D model takes into account the machine parameters and the material properties [2]. The developed model is validated using experimental tests under various operation conditions. In this work, the commercial COMSOL® software is used to solve the heat transfer equation using finite element method (FEM). The developed model is then combined to the MATLAB® software to determine the hardness profile using the metallurgical equations. The non-linear behaviour of the material is considered in that model. The FEM analysis allows taking into account the temperature dependence of certain properties like the thermal conductivity and the specific heat. The simulation is then compared and validated by experimental results. The gaps between the simulation and experimental results are statistically determined.

1.2.4-Formulation

1.2.4.1-Thermal conduction

Based on heat conduction mode, the developed models depend on the laser type and usually used the governing Fourier-Kirchhoff heat flow equation [2, 15-17]. The temperature distribution recorded at a specific time and known spatial coordinates is obtained by solving this well-known equation. Once the temperature distribution is available, the hardness profile can be determined by using metallurgical transformation equations. Ashby and Easterling established mathematical equations for metallurgical transformations during laser surface transformation of hypoeutectoid steel [5]. The most commonly used formula is the transient heat conduction equation in a solid. The heat transfer can be described by the Fourier-Kirchhoff equation.

$$\rho \times Cp \times \frac{\partial T}{\partial t} + \nabla(-K \times \nabla T) = E(x, y, z, t) \quad (1)$$

$\boldsymbol{\rho}$, C_p and K, denote, respectively, the density, specific heat and thermal conductivity of the material. x, y, z denote the Cartesian coordinates. The term $E(x, y, z, t)$ represents the heat source created by the laser beam. In this study, the heat source used for the simulation is a Gaussian beam distribution which is given by equation 2 [22].

$$E = P \times (1 - Rc) \times \frac{Ac}{2 \times \pi \times w^2} \times \mathrm{e}^{-\left(\frac{(x-(x0+V_0 \times t))^2}{2w^2} + \frac{(y-y0)^2}{2w^2}\right)} \times e^{Ac \times (Lz - z)} \quad (2)$$

w is the Gaussian beam radius, P is the laser beam power, R_c is the reflection coefficient of the surface of the material treated by laser [3], Ac is the beam power absorption coefficient [2]. V0 is the scanning speed, L_z is the part thickness and x0, and y0 are the beam center coordinates at t = 0 s. E (W/m3) represents a Gaussian heat source moving according to the x-axis at the speed V_0.

1.2.4.2-Metallurgical transformation

As the temperature in the material reaches the eutectoid temperature Ac_1, the perlite colonies transform almost instantaneously into austenite while the proeutectoid ferrite remains, assuming the initial microstructure is composed of perlite and ferrite. If it is tempered martensite, then the martensite transforms into austenite. This is the perlite dissolution into austenite (**Figure 1.1**). After the perlite colonies are transformed into austenite, the carbon diffuses outward from these transformed zones into the proeutectoid ferrite which increases the volume fraction of austenite (**Figure 1.2**). This process is called the homogenisation of austenite.

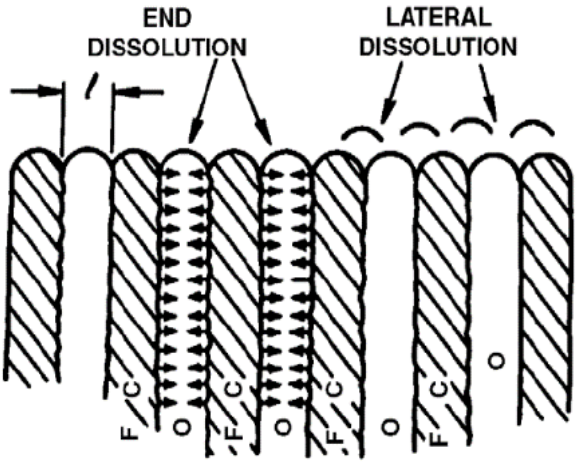

Figure 1.3 : Transformation from perlite into austenite [5]

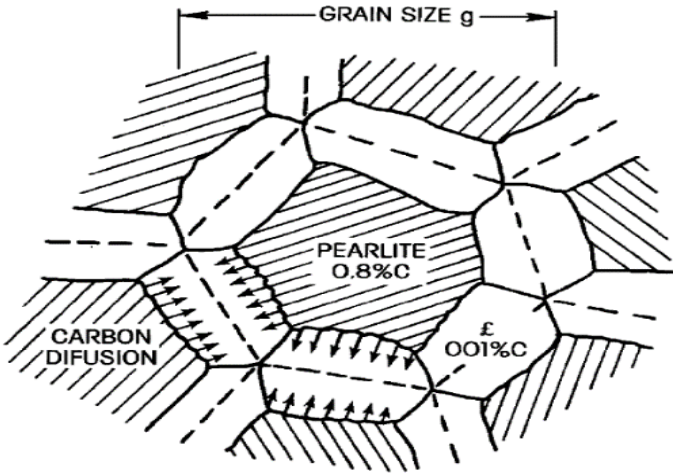

Figure 1.4 : Homogenization of hypoeutectoid steel [5]

The total number of diffusive jumps which occurs during the heat cycle affects the extent of the structural change and is given by the kinetic strength [5].

$$I=\int \exp\left\{-Q/\left(R\times T\left[t\right]\right)\right\} dt \qquad (3)$$

Q is the activation energy for the transformation and R is the gas constant. It is more convenient to express I as described in equation 4.

$$I=\alpha\tau\times\exp\left\{-Q/\left(R\times T_p\right)\right\} \quad (4)$$

Tp is the peak temperature at the considered depth and τ is the thermal time constant. The term α and τ are approximated by the equations 5 and 6.

$$\alpha=3\sqrt{\left[\left(R\times T_p\right)/Q\right]} \quad (5)$$

$$\tau=\left(1-Rc\right)P/\left(2\pi Ke^{1}V\left[T_p-T_0\right]\right) \quad (6)$$

T_0 is the initial temperature.

Ashby and Easterling established that if the perlite plate spacing is designed as "l" then for a lateral diffusion of the carbon over the distance "l" would be enough to complete the transformation from perlite into austenite and that for a heat cycle when temperature is time dependent [5].

$$l^2 = 2\times D_0\times\alpha\times\tau\times\exp(-\frac{Q}{R\times T_p}) \quad (7)$$

D0 is the diffusion constant for the carbon in ferrite.

The obtained austenite has the same carbon content as the perlite $c_e = 0.8\%$. From there, the carbon diffuses in the proeutectoid ferrite. When the temperature reaches Ac1, the volume fraction of austenite is the volume fraction f_i previously occupied by the perlite colonies (and the minimum volume fraction of martensite).

$$f_i=\left(C-C_f\right)/\left(0.8-C_f\right)\approx C/0.8 \quad (8)$$

cf is the negligible carbon content of the ferrite and c is the carbon content of the steel.

Thus, the maximum martensite fraction allowed by the transformation temperature time diagram (TTT) is

$$\begin{aligned} fm &= 0 && \text{if } T_p < Ac_1 \\ fm &= fi+(1-f_i)\times(T_p-Ac_1)/(Ac_3-Ac_1) && \text{if } Ac_1 \le T_p \le Ac_3 \\ fm &= 1 && \text{if } T_p > Ac_3 \end{aligned} \quad (9)$$

Ac_3 is the temperature of complete austenitization (**Table 1.1**).

Ashby and Easterling supposed that all the material with a specific carbon proportion more than a critical value C_c will transform into martensite. The volume fraction of the martensite is then given by equation 10 [2, 5].

$$f=fm-(fm-f_i)\times\exp\left\{-(12f_i^{2/3})/(g\sqrt{\pi})\times\ln\left[C_e/(2C_c)\right]\sqrt{(D_0\times I)}\right\} \quad (10)$$

g is the mean grain size.

The hardness can then be calculated by a mixture rule.

$$H=f\times H_m+(1-f)\times H_{f+p} \quad (11)$$

The value H_m and H_{f+p} are given by the Maynier equations that take in account the cooling rate and the composition [21].

1.2.5-Simulation

The laser heat treatment applied to an AISI 4340 50 mm x 40 mm x 5 mm parallelepiped plate is simulated with published thermal data measured at thermodynamic equilibrium. The laser has a Gaussian energy distribution in the spot created on the plate surface. The simulation efforts are performed using a 3D software. The simulation parameters considered for the modeling are the power (in W) and the scanning speed (in mm/s). The material properties behavior versus temperature is pondered in this study since finite element analysis is able to integrate the real behavior in the computation process. These physical properties are only known at thermodynamic equilibrium and transient phenomena taking place during fast heating or cooling are not taken into consideration. The material is considered as homogeneous and isotropic. The FEM analysis takes into account,

as boundary limits the ambient temperature set at 293 K. **Table 1.1** shows the material properties used for the simulation aside from the specific heat and thermal conductivity.

Table 1.1 : Material properties

Property	Symbol	Unit	Value
Reflection coefficient	Rc		0.6
Steel absorptivity	Ac	m-1	800
Eutectoid temperature	Ac1	K	996
Austenitization temperature	Ac_3	K	1053
Austenite grain size (assumed)	g	μm	10
Activation energy of carbon diffusion in ferrite	Q	kJ/mol	80
Pre-exponential for diffusion of carbon	D0	m2/s	$6x10^{-5}$
Gas constant	R	J/mol.K	8.314
Steel carbon content	C		0.43 %
Austenite carbon content	Ce		0.8 %
Ferrite carbon content	Cf		0.01 %
Critical value of carbon content	Cc		0.05 %
Volume fraction of pearlite colonies	fi		0.5375

Based on equation 2, the model is implemented using Heat transfer module of COMSOL® with x0 = 0 mm and y0 = 15 mm. The mesh is built to be fine upon the laser path and coarse elsewhere (**Figure 1.3**). A convergence study and has allowed using a suitable mesh density at the region where the laser beam heats the surface. **Figure 1.3** shows the final mesh configuration used in this study.

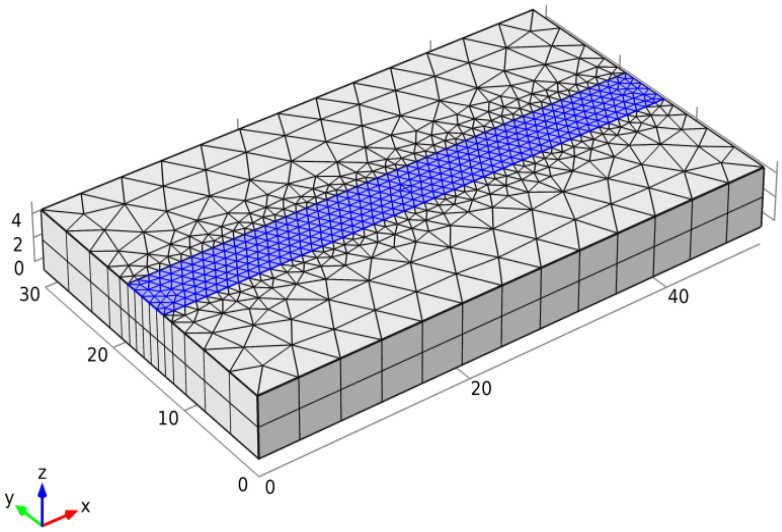

Figure 1.5 : Final used mesh (dimensions are in mm)

Figure 1.4 shows the effect of mesh quality on the obtained temperature. The temperature TA, TB and TC are chosen to have a representation of the temperature distribution at the surface. The three points have the same coordinate according to the x-axis (25 mm) and the same coordinate according to the z-axis (5 mm). According to the y-axis, the three measurement locations A, B and C are at 12.5 mm, 15 mm and 17.5 mm respectively. The temperature TB is at the surface directly on the middle plan where the laser beam is in contact with the surface. The temperatures TA and TC are positioned symmetrically across the middle plan. Due to the symmetry appearance, these temperatures should display the same value. The convergence curves demonstrate that the temperatures become unchanged between the size mesh of 0.6 mm and 1.1 mm. In the outside of this range, the temperatures fluctuate due to the accuracy and truncation errors.

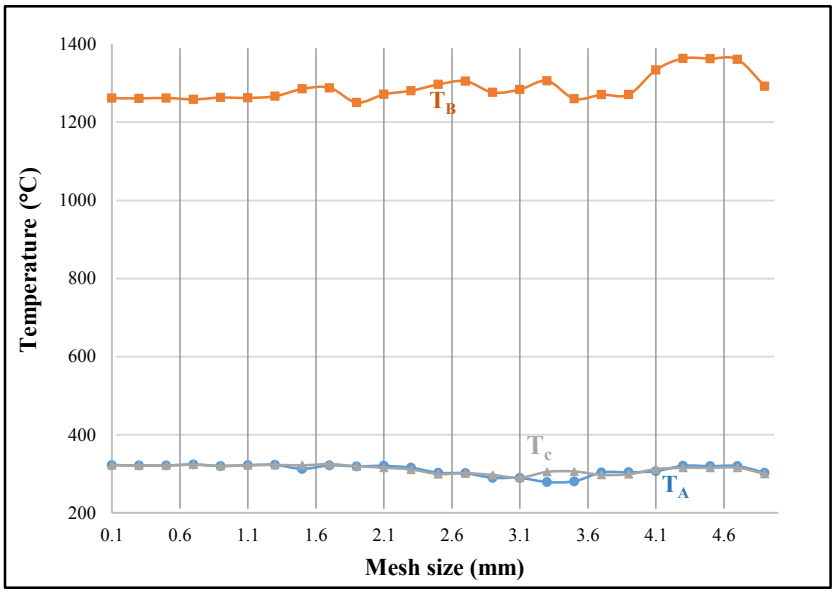

Figure 1.6 : Effect of mesh size on obtained temperatures

The final mesh size that is chosen is 1.1 mm upon the laser path and is a good compromise between accuracy and computation time. The input power, scanning speed and reflection coefficient of the surface can be freely arranged. The simulation takes into account the emissivity of the surfaces as well as the heat convection phenomenon through the surfaces to the ambient air. The obtained results are developed at specific process parameters for the beginning in order to understand the effect and to present the temperature distribution.

For this purpose, the power is fixed at 1200 W and the scanning speed at 15 mm/s. The simulation results show that the temperature reach high values in the region near to the spot path and decreases drastically away from it. To illustrate the temperature behavior, 3 cases are exposed. **Figure 1.5, Figure 1.6 and Figure 1.7** show the isothermal contours at 1 s, 2 s and 3 s respectively. At the beginning (**Figure 1.5**), at the beam spot center, high value of temperature are recorded (above 1100 °C) and the generated heat remains concentrated around the spot. At the end of the heating cycle (3 s), high values of temperature are still recorded at the beam spot center. However, the part becomes globally heated with more heat amount due to the conduction. Some heat is lost by convection and radiation modes through the surface but the major part created by the laser is absorbed by

the part by conduction. The fact that the laser concentrates the power in a small area generates a very high heat flux with high temperature gradient. It affects the metallurgical transformation especially in the region around the spot beam. Once heated, this region could reach melting point and the hardness profile will include a small non desirable melting layer. However, the part volume presents an industrial advantage since it acts as a cooler to transform the region heated above the Ac_3 directly to hard martensite without a forced convection.

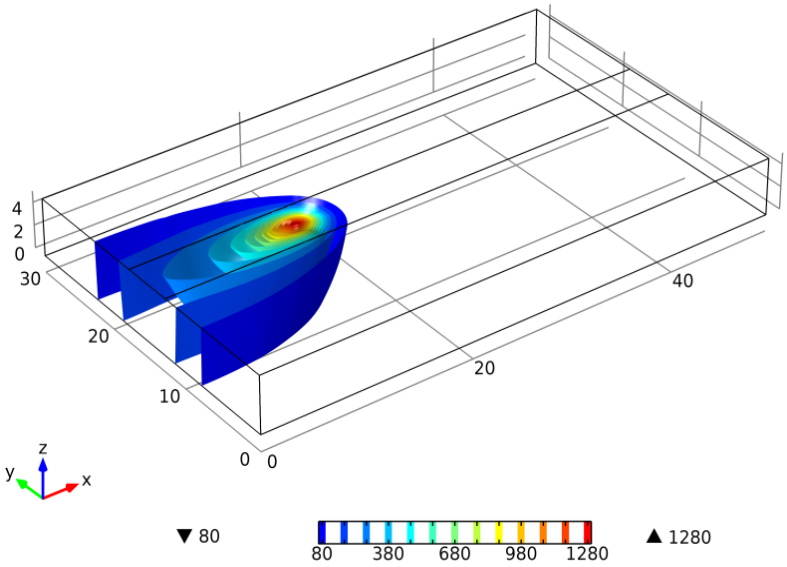

Figure 1.7. Isothermal contours of temperature (t = 1 s)

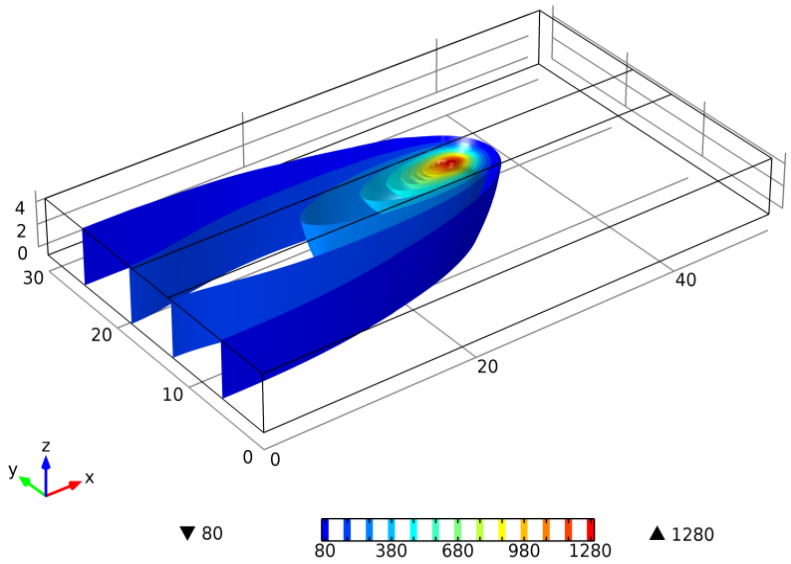

Figure 1.8. Isothermal contours of temperature (t = 2 s)

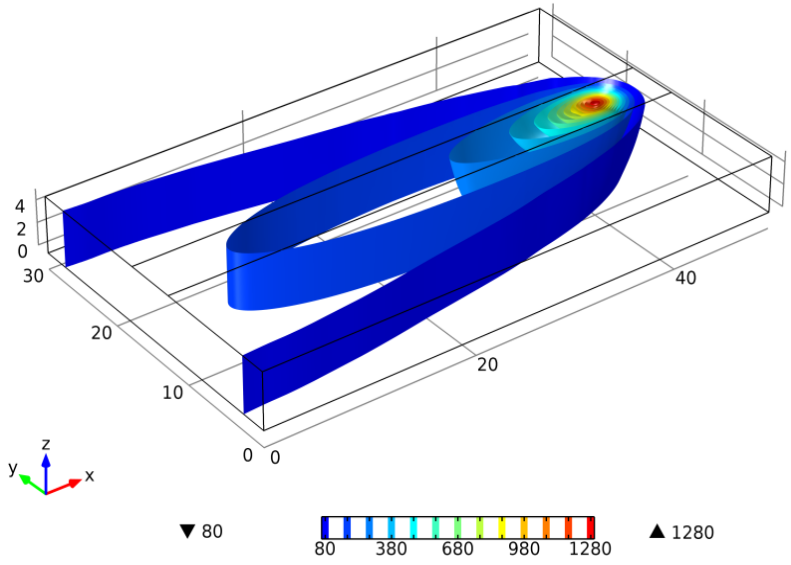

Figure 1.9. Isothermal contours of temperature (t = 3 s)

Figure 1.8 shows the temperature evolution depending on the time at different depths under the surface. The temperature curves are compared to Ac_1 and Ac_3 temperatures to approximate the case depth. The temperature rapidly increases to reach a maximum value of 1050 °C before dropping off. The temperature profile shows that the

temperature is important at the surface and decreases with the depth. At only 3 mm depth, the temperature at the same time (1 s) is three times lower. The figure also shows that the cooling rate is extremely high which is essential for the martensite to be formed. In the case of AISI 4340, the time taken to drop at a low temperature is well within the limit of the TTT diagram which ensures the formation of the hard martensite microstructure due to its high hardenability. A first approximation could confirm that the case depth is between 0.7 mm and 1.4 mm for the chosen process parameters.

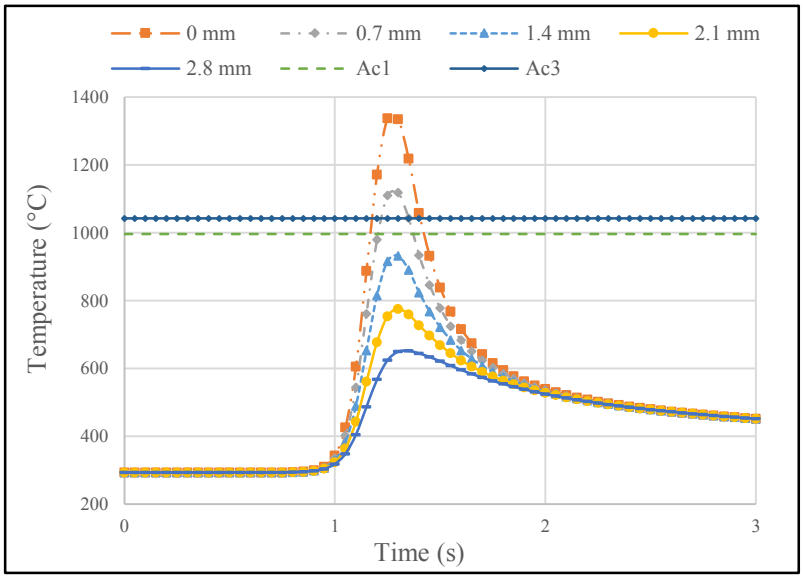

Figure 1.10 : Temperature versus time for various depths measured from heated surface at middle plan

Figure 1.9 shows the Gaussian temperature profile along the y-axis at a given time and at different depths and the comparison with the temperatures Ac_1 and Ac_3. It can be seen that away from the middle axis (beam spot center), the region heated beyond the austenitization temperature Ac_3 becomes smaller. Under the midpoint, the case depth is about 1.5 mm but it is only 0.5 mm if a 1.3 mm shifted point to the left or to the right is considered. The assumption stipulates that all austenitized regions become martensite upon cooling. In fact, the used steel is recognized to have a good hardenability [23]. The case depth is about 1 mm in this case.

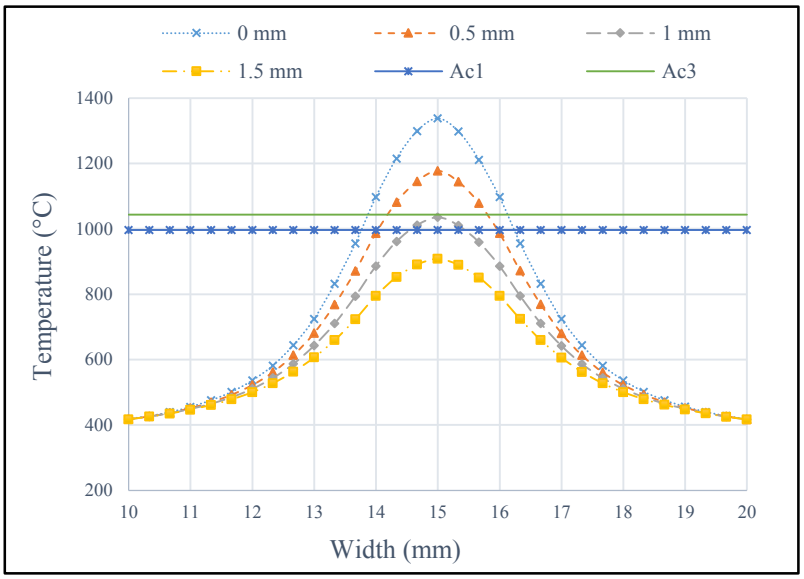

Figure 1.11 : Temperature profile along the y-axis at a given time and at different depths

1.2.6-Validation

To validate the developed model, a 3 kW laser power is used (IPG YLS-3000-ST2). The laser is equipped with a 6 degrees of freedom articulated robot. The experimental setup is illustrated in **Figure 1.10**. The plate is placed according a referential coordinates systems. In order to be at the maximum power focus, the upper surface of the plate is adjusted vertically to match the focal distance. The laser beam diameter is evaluated at 1.08 mm when focused. The focal distance is 310 mm with permissible tolerance of ± 5%. The programmed tests consist of heating the surface with chosen scanning speed and power to generate a martensitic transformation within a specific case depth more than 0.5 mm. At each distinct test, the laser beam travels a distance of 40 mm along the plate length. Once the treatment is carried out and the samples are prepared and polished, a micro-hardness measurement allows characterizing the hardness curve as a function of the depth using a Clemex® micro-hardness machine.

Prior to the laser heat treatment, the samples are oil-quenched then tempered in a furnace at 510 °C during 1 hour. As a result, the initial microstructure is a tempered

martensite with hardness about 400 HV. In the case of AISI 4340, the tempering treatment before the laser heat treatment has been proved to have a huge impact on the final hardness profile. For steels tempered at a high temperature, the over tempered zone, where the hardness of the steel is inferior to the core hardness of the material (and which is generally undesirable), will be minimized [8].

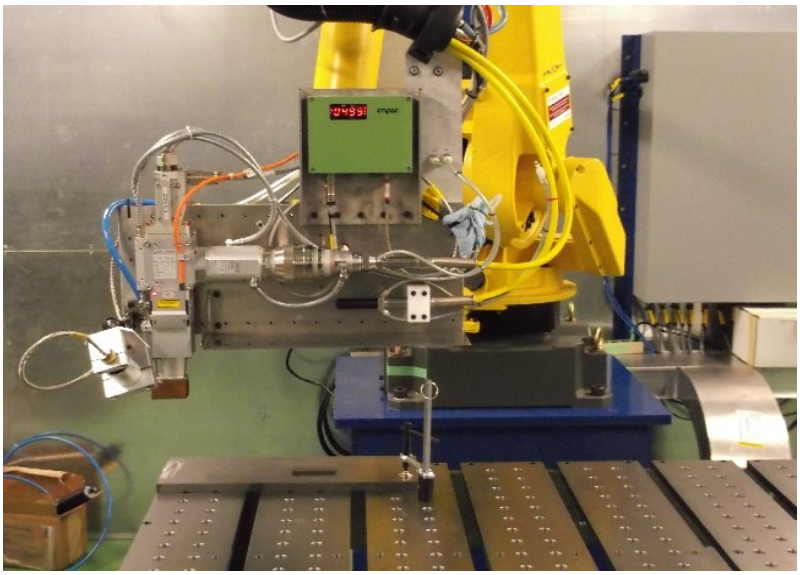

Figure 1.12 : Experimental setup

The validation test is based on a factorial design composed of 2 factors at 2 levels. The first factor is the laser beam power and it is varying from 950 W to 1100 W. The second factor is the scanning speed varying from 16 mm/s to 18 mm/s. **Table 1.2** shows the experimental matrix (L4) for laser hardening validation.

Table 1.2 : Experimental matrix for validation

Test	Power (W)	Scanning speed (mm/s)
1	950	16
2	950	18
3	1100	16
4	1100	18

Figure 1.11 shows a transverse section of the laser-hardened zone. As expected of a Gaussian distribution where the energy is higher at the center of the laser beam spot, an

elliptic section can be observed. The case depth is approximately 0.72 mm and the width of this region is 2.34 mm. The hardened region can be divided in melting and hard region.

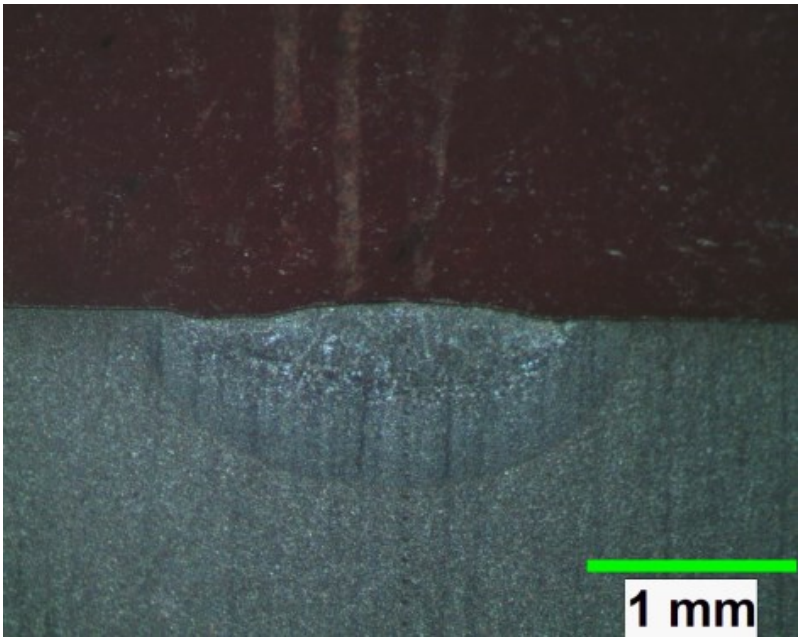

Figure 1.13 : Metallographic picture of hardness profile - Test 2

Figure 1.12 to **Figure 1.15** show the predicted and measured hardness curves. To describe the hardness evolution versus the depth, the core hardness H_{f+p} is replaced by the material core hardness (400 HV). It is important to note that even with an initial tempered martensitic microstructure instead of an initial perlite microstructure, the measured hardness is always in average within a 15% uncertainty of the predicted value as shown in **Table 1.3**. The case depth hardened is between 0.7 mm for the set of parameters 950 W and 18 mm/s. The case depth is evaluated at 1.05 mm for a power of 1100 W and a scanning speed of 16 mm/s. As expected, the case depth seems to increase when the laser power increases or the scanning speed is reduced. It is relevant to remark that, each time, just before the transition where the hardness drops; there is a small area where the hardness is higher than it is just below the surface. In fact, the surface hardness is not maximal since

this region is melted. The hardness continues to increase with the depth to reach maximal value or hard martensite before dropping off.

After this area, there is another area called the over-tempered zone which has not been treated but has been nonetheless affected by the heat and softened. In this area, the hardness is less than it is in the core material. Usually unwanted, the size of this zone depends on the initial microstructural properties [8]. However, the model used in this study is unable to predict the two precedent areas that are observed for all the tests conducted in this study.

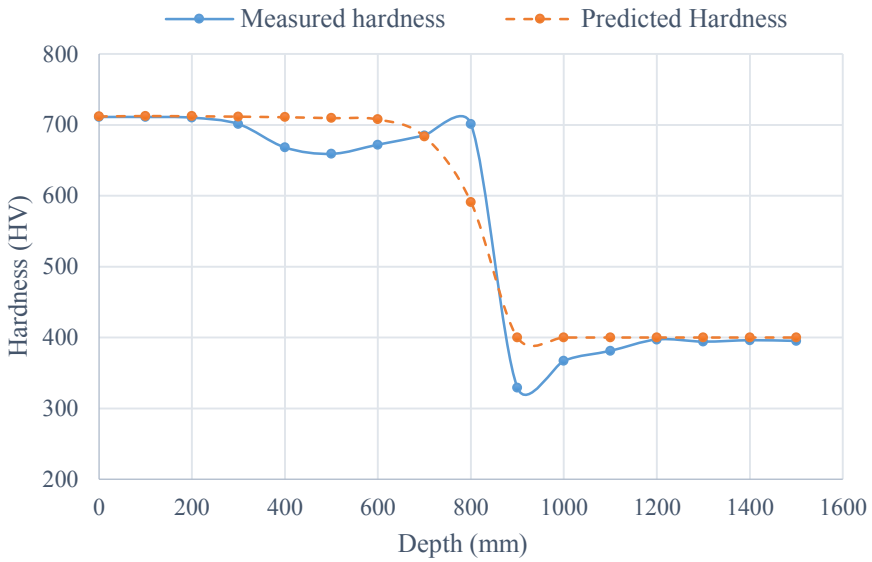

Figure 1.14 : Hardness curve for test 1 (950 W and 16 mm/s)

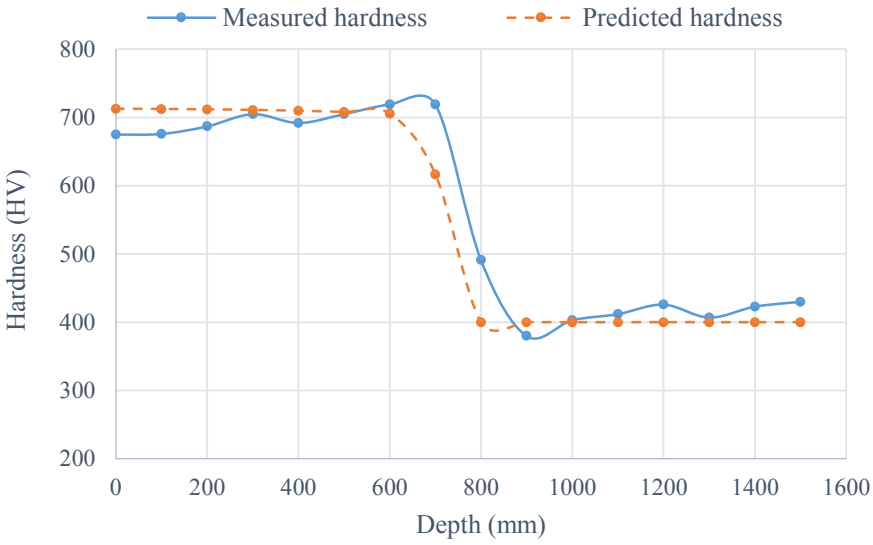

Figure 1.15 : Hardness curve for test 2 (950 W and 18 mm/s)

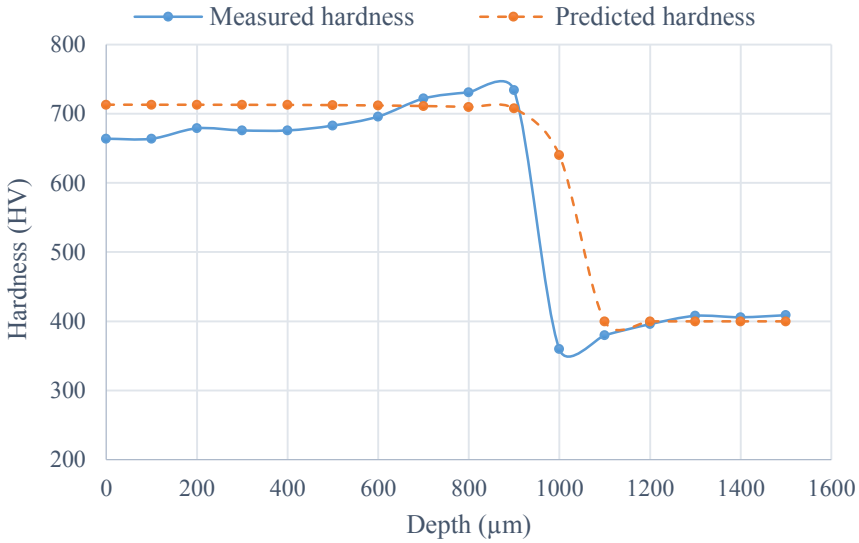

Figure 1.16 : Hardness curve for test 3 (1100 W and 16 mm/s)

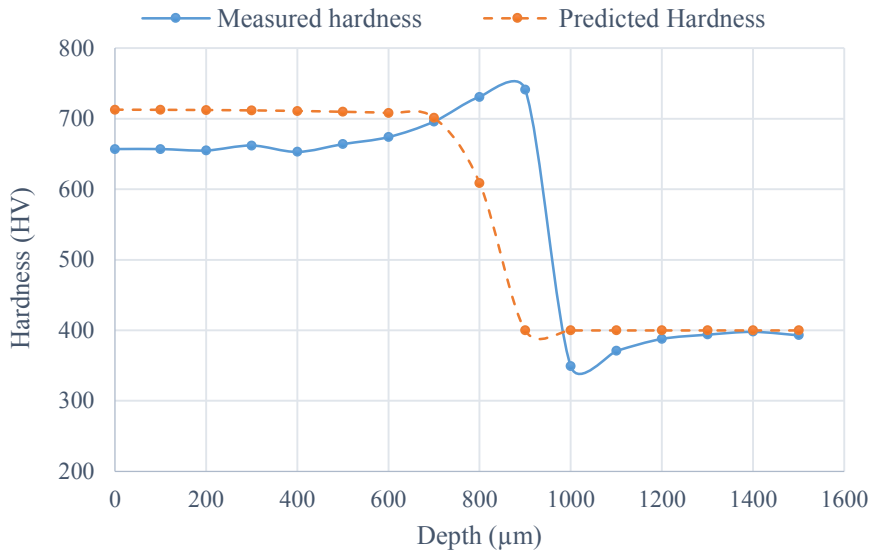

Figure 1.17 : Hardness curve for test 4 (1100 W and 18 mm/s)

In **Figure 1.14** and **Figure 1.15**, It can be seen that the measured hardness under the surface is less than the predicted hardness (a difference of 40 HV approximately). This gap can be explained by the fact that the temperature just under the surface most likely reached the melting point during the experiments with a power of 1100 W due to the fact that the reflection coefficient is a bit lower than predicted. For each experiment, the maximum relative error seems to be high but this only is because the model is unable to predict the hardness in the over tempered zone which results in a located big gap between the simulated hardness and the measured hardness in this zone. However, as the mean relative error testifies, for each test, the rest of the predicted hardness profile fairly matches the measured profile (**Table 1.3**).

Table 1.3 : Average absolute and relative hardness errors

	Absolute error (HV)	Relative error (%)
Test 1	25	4.9
Test 2	28	5.1
Test 3	40	8.4
Test 4	58	9.2

Table 1.4 shows the comparison between hardened depths for each experiment. Because the reflection coefficient is difficult to determine with a good accuracy and it has an impact on the case depth, some small differences can be observed between measured case depth and simulated case depth. As the drop of hardness is very fast in the transition zone, even an error of 0.1 mm between simulated case depth and measured case depth leads to a big gap between simulated hardness and measured hardness in this zone which can be especially seen on **Figure 1.15**. The absolute difference between the measured depth and the predicted depth is less than 0.1 mm for each case. The model can predict the case depth with maximal relative error of 14.3 %.

Table 1.4 : Comparison of hardened depth

	Measured case depth (mm)	Predicted case depth (mm)	Relative error (%)
Test 1	0.8	0.7	-12,5
Test 2	0.7	0.6	-14,3
Test 3	0.9	1.0	-11,1
Test 4	0.9	0.8	-11,1

1.2.7-Conclusion

In this study, a laser heat treatment applied to AISI 4340 steel is modeled using a FEM commercial software. The model generates successfully numerical solutions of the heat-flow equation and gives a complete simulated 3D temperature distribution in the laser-hardened sample. It allows an accurate prediction of the hardness profile without doing any experiments. As seen in the validation paragraph, the generated model fairly matches both the actual hardness and the depth. A maximum hardness of 734 HV with a case depth of 1.05 mm is obtained in these experiments. However, both the simulation and the experiment show that the input power and the scanning speed must be carefully chosen in order to harden a part on a satisfying depth without reaching the melting point at the surface of the material. The obtained results will be advantageously exploited to determine the sensitivity of the developed model using statistical tools within large range of variation of the model.

CHAPITRE 2
MODÈLE DE RÉSEAU DE NEURONES ARTICFICIELS POUR L'ESTIMATION DU TRAITEMENT THERMIQUE SUPERFICIEL AU LASER D'UNE PLAQUE D'ACIER 4340

2.1-RESUME EN FRANÇAIS DU DEUXIEME ARTICLE

L'article se concentre sur l'amélioration du modèle développé dans le premier article afin de le rendre plus robuste en vue du passage plus aisé à des géométries complexes. Il s'agit d'utiliser l'équation de la chaleur afin de déterminer la distribution thermique dans le matériau pendant le traitement puis de déterminer le profil de dureté grâce aux équations d'Ashby et Easterling. La différence avec le premier article est qu'ici, la source de chaleur est remplacée par un flux de chaleur plus proche de la réalité d'un faisceau laser. Cette nouvelle approche est vérifiée par la suite avec des tests expérimentaux. De plus, l'article aborde une utilisation ultérieure des données (profondeurs et largeurs durcies) générées par le modèle. En effet, une fois le modèle numérique mis en place et vérifié expérimentalement, il permet d'effectuer un grand nombre de simulations avec des paramètres d'entrée différents. Ce grand nombre de données permet de réaliser des études statistiques très précises et fiables (notamment sur les effets relatifs des paramètres sur le résultat du traitement thermique superficiel au laser). En outre, ces résultats permettent d'entrainer un réseau de neurones artificiels qui peut alors fonctionner indépendamment d'un logiciel de calcul par éléments finis et donner instantanément le résultat d'un traitement thermique superficiel au laser pour un ensemble de paramètres donné.

Ce deuxième article, intitulé «*ANN Based Model for Estimation of Transformation Hardening of AISI 4340 Steel Plate Heat-Treated by Laser*», fut rédigé par moi-même ainsi

que par les professeurs Noureddine Barka et Abderrazak El Ouafi. Il fut accepté pour publication dans sa version finale en 2015 par le « Journal of Materials Sciences and Applications (MSA) ». En tant que premier auteur, ma contribution à ce travail fut l'essentiel de la recherche sur l'état de l'art, le développement de la méthode, l'exécution des tests de performance et la rédaction de l'article. Les professeurs Abderrazak El Ouafi et Noureddine Barka, respectivement second et troisième auteur, ont fourni l'idée originale. Ils ont aidé à la recherche sur l'état de l'art, au développement de la méthode ainsi qu'à la révision de l'article.

2.2- ANN BASED MODEL FOR ESTIMATION OF TRANSFORMATION HARDENING OF AISI 4340 STEEL PLATE HEAT-TREATED BY LASER

G. Billaud
Mathematics, Computer Science and Engineering Department
University of Quebec at Rimouski
Rimouski, Canada, G5L 3A1

A. El Ouafi
Mathematics, Computer Science and Engineering Department
University of Quebec at Rimouski
Rimouski, Canada, G5L 3A1

N. Barka
Mathematics, Computer Science and Engineering Department
University of Quebec at Rimouski
Rimouski, Canada, G5L 3A1

2.2.1-Abstract

Quality assessment and prediction becomes one of the most critical requirements for improving reliability, efficiency and safety of laser surface transformation hardening process (LSTHP). Accurate and efficient model to perform non-destructive quality estimation is an essential part of the assessment. This paper presents a structured and comprehensive approach developed to design an effective artificial neural network (ANN) based model for quality estimation and prediction in LSTHP using a commercial 3 kW Nd:Yag laser. The proposed approach examines laser hardening parameters and conditions known to have an influence on performance characteristics of hardened surface such as hardened bead width (HBW) and hardened depth (HD) and builds a quality prediction model step by step. The modeling procedure begins by examining, through a structured experimental investigations and exhaustive 3D finite element method simulation efforts, the relationships between laser hardening parameters and characteristics of hardened surface and their sensitivity to the process conditions. Using these results and various statistical tools, different quality prediction models are developed and evaluated. The results demonstrate that the ANN based assessment and prediction proposed approach can effectively lead to a consistent model able to accurately and reliably provide an appropriate

prediction of hardened surface characteristics under variable hardening parameters and conditions.

Keywords: Laser hardening process, AISI 4340 steel, case depth, hardened bead width, artificial neural network.

2.2.2-Introduction

In the industry, many steel components require a surface heat treatment in order to have the desired surface qualities such as hardness and wear resistance. Among the available processes, laser hardening process (LHP) is one of the most efficient, as it allows a very fast and localized metallurgical transformation. In addition, the process generates a hard surface layer with low distortion [2]. Using high energy beam, the surface is rapidly heated to reach the transition temperatures (microstructure changes) before being quenched by heat conduction into the colder core of the material. Consequently, a martensitic layer is produced without affecting the core of the material [3].

Despite its industrial advantages, predicting hardness profiles with a good accuracy remains difficult. Indeed, besides the process parameters (Power, scanning velocity and focus diameter), which can be properly set, the process is affected by the non-linear behavior of thermo-physical and metallurgical properties of the material [2]. It makes the temperature distribution uneasy to predict by complicating the resolution of the governing heat-flow equation. Experimental tests are also expensive in terms of time and resources, especially if one wants to test many combinations of control parameters to have a better understanding of the process.

Among all the approaches that can be used to understand the process and ultimately to predict its performance, 3D simulation represents a powerful tool for combining multi-physics problems and taking into account the material and complex geometries. In fact, the developed model includes the non-linear properties of the material and the heat-flow equation is solved using the finite element method (FEM) [14, 17]. The FEM enables

solving the governing heat-flow equation that determines the temperature distribution for each time step during the heating process. The hardness is then approximated by the equations of Ashby and Easterling [5]. The advantage of the simulation is that, although it might be long and tedious to implement, once it is completed and experimentally verified in a few cases, one can test any combination of input parameters and quickly generate a large number of data which can be used for further exploitation. Many studies have been conducted to optimize the various laser process parameters (surface hardening, laser welding, laser cutting, etc.) through statistical methods such as the ANOVA method. It can be applied in many fields of engineering, including production processes and products for professional and consumer markets all over the world [19]. S-L Chen and D. Shen [24] used the Taguchi tools such as graphic designs of parameters and analysis of variance (ANOVA) to optimize the hardened depth (HD) and the hardened bead width (HBW) in the case of the LHP. Badkar and Pandey [20] used the same tools to determine the relative importance of each parameter on the LHP. K.Y. Bentounis, A.G. Olabi and M.S.J. Hashmi [25] conducted a similar study in the case of a laser welding process. Most recently, Sathiya et al. [26] also used the Taguchi method to optimize the laser welding parameters. Given that experimental characterization requires great efforts in terms of time and money, it is not easy to experiment all the combinations of the input parameters. The Taguchi method really is an asset, as it is a partial factorial design that only requires some combinations of the input parameters in order to be performed and yet, it gives accurate statistical results in the overall process.

Others studies are conducted using artificial neural networks (ANN) in order to improve the performance of the laser processes [27]. Ciurana J. et al. [28] used ANNs to establish a model for laser micromachining of hardened steel and to optimize the process parameters. Pan Q.Y et al. [29] performed a similar study by using a neural network to model the non-linear relationship between laser processing parameters and corrosion resistance of the surface of stainless steel during the process of laser surface re-melting, which locally improved the corrosion resistance of the steel. Munteanu and Adriana [30] predicted the surface hardness of steel using a neural network in the case of an electron

beam machining process which is similar to the LHP. F. Lambiase et al. developed a prediction model of laser hardening by means of an ANN using experimental datasets and linear interpolations between those experimental measures to train the network. However, to obtain good and efficient modeling results with ANN techniques, a large quantity of experimental data is advantageous and the observations should cover a sampling space as wide as possible in order to simplify the interpolation task.

Indeed, in any modelling experiment, the results depend, to a large degree, on the method used to collect data. In a lot of cases, full factorial experiments are conducted. This approach cannot be implemented when too many factors are under consideration, because the number of repetitions required would be prohibitive in time and cost. Regular fractional factorial designs cannot produce credible results when interactions among the factors exist. By contrast, the use of a testing strategy such as the orthogonal arrays (OAs) developed by Taguchi leads to an efficient and robust fractional factorial design of experiments that can collect all the statistically significant data with a minimum number of repetitions. Accordingly, OAs are used in this study for the experimental design. On the other hand, by using 3D FEM simulation that can provide results matching fairly well with the experimentally observed variables, one can easily and quickly obtain additional data for any combination of input parameters. The quantity of simulated data generated in a short time compared to experimental data would allow exhaustive statistical analysis including all levels of all input parameters. Moreover, with a large quantity of data for training, a simple Multilayer Perceptron ANN can be appropriate for modeling.

The objective of this paper is to presents a structured and comprehensive approach developed to design an effective artificial neural network (ANN) based model for quality estimation and prediction in LSTHP using a commercial laser source. The proposed approach examines laser hardening parameters and conditions known to have an influence on performance characteristics of hardened surface such as hardened bead width (HBW) and hardened depth (HD) and builds a quality prediction model step by step. The modeling procedure begins by examining, through a structured experimental investigations and

exhaustive 3D FEM simulation efforts, the relationships between laser hardening parameters and characteristics of hardened surface and their sensitivity to the process conditions. Using these results and various statistical tools, different quality prediction models are developed and evaluated. In order to carry out the models building procedure, an efficient modeling planning method combining neural networks paradigm, a multi-criteria optimization and various statistical tools is adopted.

2.2.3-3D Model implementation and validation

2.2.3.1-Implementation

The 3D FEM model is developed on the commercial software to estimate the temperature profiles. These temperature profiles are used to approximate the surface hardness profiles (surface hardness, HD, HBW). The part is a 50 mm × 30 mm × 5 mm parallelepiped (**Figure 2.1**).

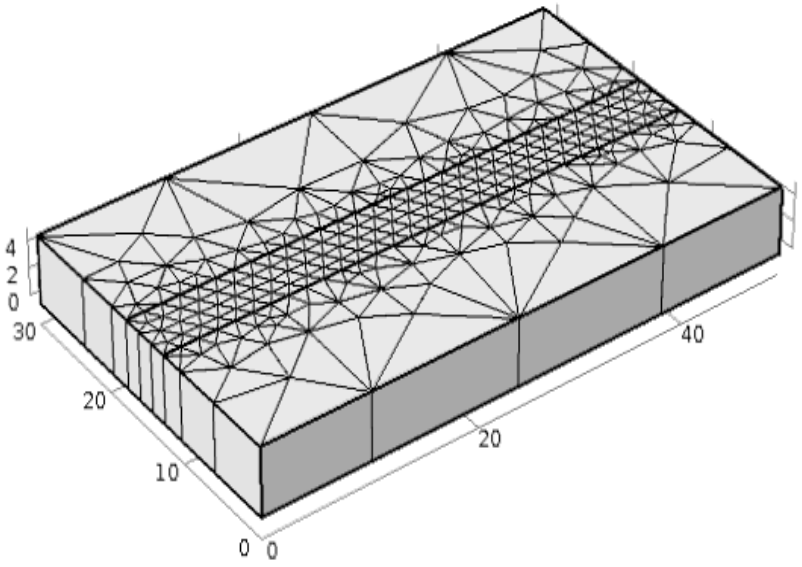

Figure 2.1 : Sample with its mesh implemented on COMSOL

In this study, the heat flux used for the simulation is considered as a Gaussian beam distribution type which is given by equation 1 [2],

$$E=E_0\times\exp\{-([x-(x_0+V\times t)]^2/(2w^2)+[y-y_0]^2/(2w^2))\} \quad (1)$$

Where V is the scanning velocity, and x0 and y0 are the beam center coordinates at t = 0 s. E (W/m2) represents a Gaussian heat flux moving according to the x-axis at the velocity V. E_0 is defined by equation 2,

$$E_0=P(1-Rc)/(2\pi w^2) \quad (2)$$

Where w is the Gaussian beam radius, P is the laser beam power, Rc is the reflection coefficient of the material surface [3].

The moving isothermal contours can be observed in **Figure 2.2**. Because of the Gaussian form of the beam, the temperature is at its maximum (about 1110 K) at the center of the spot. The temperature decreases rapidly with the depth because of heat conduction into the colder core of the material. The heated volume is small at the beginning of the process (t = 0.4 s) and it gets larger as the time passes and the beam moves (t = 2.5 s). As it can be seen in **Figure 2.2**, the small volume of the part that had reached the temperature of 1110 K at t = 0.4 s (see **Figure 2.2.a**) cool downed to reach a temperature under 430 K at t = 2.5 s (see **Figure 2.2 b**). It means that a very fast quenching happened in that volume.

Once the temperature distribution is determined, the hardness profile is estimated using the equations of Ashby and Easterling [5]. Those equations are implemented in MATLAB® to obtain the hardness at any point belonging to the heated part and, consequently, the hardness curve representing the hardness versus depth.

The 4340 steel properties are displayed in **Table 2.1**.

The specific heat and the thermal conductivity are temperature dependant and their dependency is taken into account in our model.

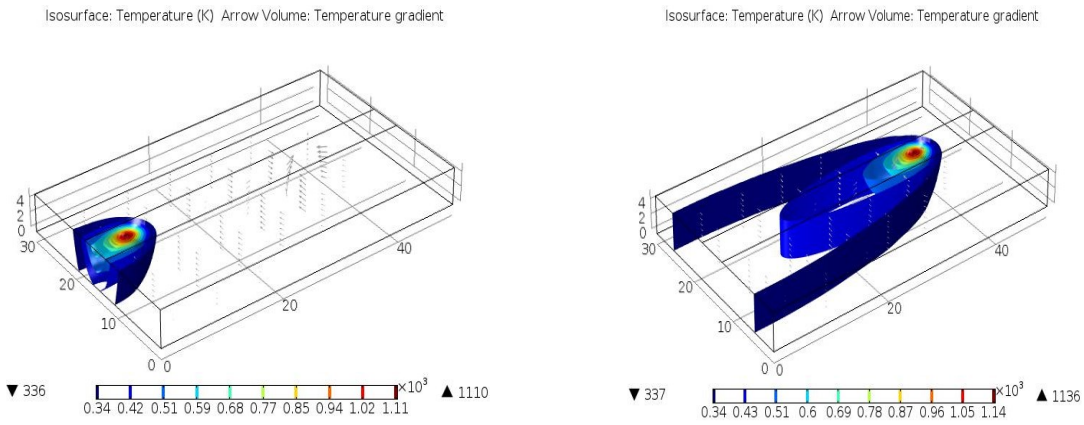

(a) (b)

Figure 2.2 : Isothermal contours: (a) --» t = 0.4 s and (b) --» t = 2.5 s

Table 2.1 : Metallurgical properties

Property	Symbol	Unit	Value
Reflection coefficient	Rc		0.6
Eutectoid temperature	Ac1	K	996
Austenitization temperature	Ac3	K	1053
Austenite grain size (assumed)	g	µm	10
Activation energy of carbon diffusion in ferrite	Q	kJ/mol	80
Pre-exponential for diffusion of carbon	D0	m^2/s	$6x10^{-5}$
Gas constant	R	J/mol.K	8.314
Steel carbon content	C		0.43 %
Austenite carbon content	Ce		0.8 %
Ferrite carbon content	Cf		0.01 %
Critical value of carbon content	Cc		0.05 %
Volume fraction of pearlite colonies	fi		0.5375

2.2.3.2-Metallurgical equations

When the temperature in the material reaches the eutectoid temperature Ac_1 in a small volume under the surface, the steel microstructure, which is generally tempered martensite in the case of the steel AISI 4340, starts to transform into austenite. The complete transformation from tempered martensite to austenite occurs when the temperature reaches Ac_3. In the case of laser hardening treatment, when the temperature drastically decreases

due to rapid heat diffusion into the colder core of the part, the austenite transforms into hard martensite. This is what is called a heat cycle (**Figure 3**).

As seen on **Figure 3**, the peak temperature at the surface is above Ac_3. Therefore, a complete transformation into hard martensite happened at the surface. However, the peak temperature at 1.4 mm under the surface is under Ac_1. It means that no transformation happened at this depth.

The total number of diffusive jumps that occur during the heat cycle affects the extent of the structural change and is given by the kinetic strength I [2, 5],

$$I = \int \exp\left\{-Q/\left(R \times T\left[t\right]\right)\right\} dt \tag{3}$$

Where Q is the activation energy for the transformation and R is the gas constant. It is more convenient to express I as described in equation 4.

$$I = \alpha \times \tau \times \exp\left\{-Q/\left(R \times T_p\right)\right\} \tag{4}$$

Here Tp is the peak temperature at the considered depth and τ is the thermal time constant. The terms α and τ are approximated by equation 5 and 6,

$$\alpha = 3\sqrt{\left[\left(R \times T_p\right)/Q\right]} \tag{5}$$

$$\tau = \left(1\text{-}Rc\right) \times P/\left(2 \times \pi \times K \times e^1 \times V \times \left[T_p\text{-}T_0\right]\right) \tag{6}$$

Where T_0 is the initial temperature.

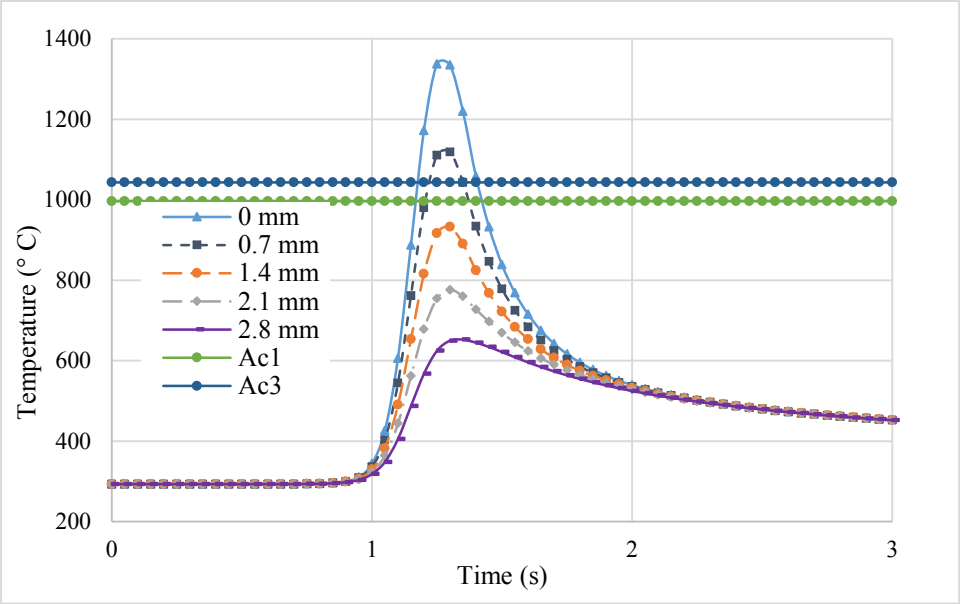

Figure 2.3 : Temperature evolution at different depths (850 W and 9 mm/s)

The obtained austenite has the same carbon content as a perlite microstructure C_e = 0.8 %. From there, the carbon diffuses into the proeutectoid ferrite. When the temperature reaches Ac_1, the volume fraction of austenite is f_i (which is also the minimum volume fraction of martensite), given by equation 7,

$$f_i = (C-C_f)/(0.8-C_f) \approx C/0.8 \qquad (7)$$

Where C_f is the negligible carbon content of the ferrite and C is the carbon content of the steel.

The maximum martensite fraction allowed by the transformation temperature time diagram (TTT diagram) is

$$\begin{aligned} fm &= 0 && \text{if } T_p < Ac_1 \\ fm &= fi+(1-f_i)\times(T_p-Ac_1)/(Ac_3-Ac_1) && \text{if } Ac_1 \le T_p \le Ac_3 \\ fm &= 1 && \text{if } T_p > Ac_3 \end{aligned} \qquad (8)$$

Ashby and Easterling supposed that all the material with a specific carbon proportion above the critical value C_c will transform into martensite. The volume fraction of the martensite is then given by equation 9 [2, 5].

$$f = fm-\left(fm-f_i\right)\times\exp\left\{-\left(12\times f_i^{2/3}\right)/\left(g\times\sqrt{\pi}\right)\times\ln\left[C_e/\left(2\times C_c\right)\right]\sqrt{\left(D_0\times I\right)}\right\} \quad (9)$$

Here g is the mean grain size and D_0 is the diffusion constant for the carbon in ferrite.

The hardness can then be calculated by a mixture rule (equation 10).

$$H=f\times H_m+\left(1-f\right)\times H_{f+p} \quad (10)$$

The value H_m and H_{f+p} are given by Maynier equations that take in account the cooling rate and the composition of the material [21].

2.2.4-Experimental validation

The experimental procedure consists of a first heat treatment in a furnace with a water quenching followed by a tempering at 640 °C for 1 hour. The aim is to reach a homogeneous hardness of 440 HV for all the samples. Then, a commercial 3 kW Nd:Yag laser power (IPG YLS-3000-ST2), combined with a 6 degrees of freedom articulated robot (**Figure 2.4**) is used to perform laser heating. The plan-parallel sample is put on a metal plate under the laser head. This type of laser generates a laser beam with a wavelength λ = 1064 μm. The process parameters are the input power, the scanning velocity and the focus diameter. In this study, the laser beam has a straight-line trajectory as seen in **Figure 2.2**. Finally, the resulting case depth is measured by micro indentation.

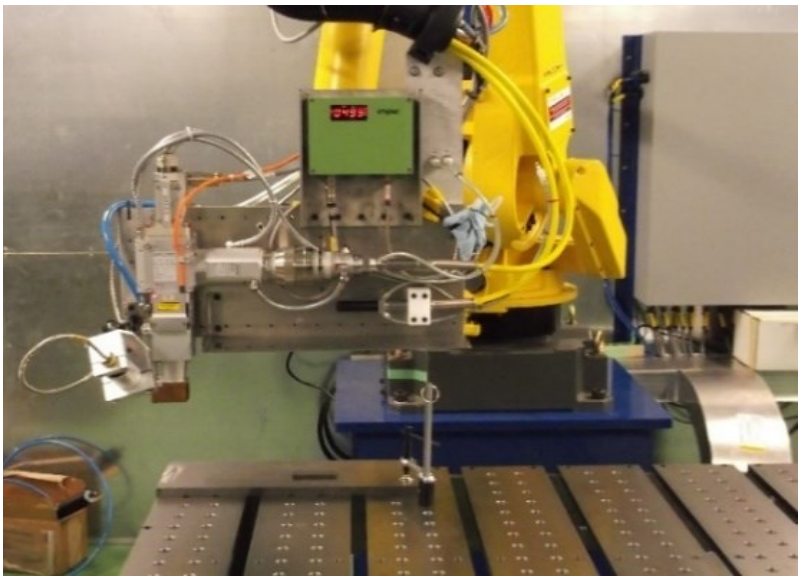

Figure 2.4 : Experimental setup for model validation

Experimental validations are conducted according the **Table 2.2**. The focus diameter is 1260 µm for the three tests. The values are chosen so that the surface temperature reaches the austenite temperature Ac_3 but does not hit the melting temperature (about 1450 °C).

Table 2.2 : Experimental matrix for validation

Test	Power (W)	Scanning velocity (mm/s)
1	850	9
2	850	12
3	950	12

A micro-hardness machine is used to characterize the hardness curve as a function of the depth. After the laser treatment, the samples are prepared and polished to reach adequate surface finish. The hardness is then measured by using a micro-hardness machine. The validation is conducted by micro indentation, with 100 µm steps between consecutive Vickers marks on the surface along a vertical axis. The experimental results help to validate and calibrate the model. In this sense, the obtained results confirm the concordance between the experimental and simulated hardness curves. This suggests that even if the developed model is not able to accurately predict the hardness curve, it can determine the hardened depth with good accuracy. **Figures 2.5**, **Figure 2.6** and **Figure 2.7** show a

comparison between the simulated and measured hardness curve using Vickers hardness scale (VH) for the three tests (**Table 2.2**). It is worth noting that the developed 3D model is unable to predict the over-tempered zone where the hardness of the material becomes inferior to the initial hardness. However, hardened zone, transition zone and unaffected zone are correctly predicted. As expected, the hardened depth (at the start of the transition zone) increases as the power rises and/or the scanning velocity decreases. **Table 2.3** shows the average absolute and relative errors between measured and simulated hardness. The preliminary tests allow to conclude that, despite the difference of more than 50 HV in terms of absolute error, the relative error is very small, not exceeding 10 %. As shown in **Figure 2.5**, **Figure 2.6** and **Figure 2.7**, the simulation is fairly accurate in both hardness prediction and case depth prediction.

Table 2.3 : Average absolute and relative hardness errors resulting from the preliminary tests

Test	Absolute error (HV)	Relative error (%)
1	43	8.8
2	30	5.2
3	24	4.0

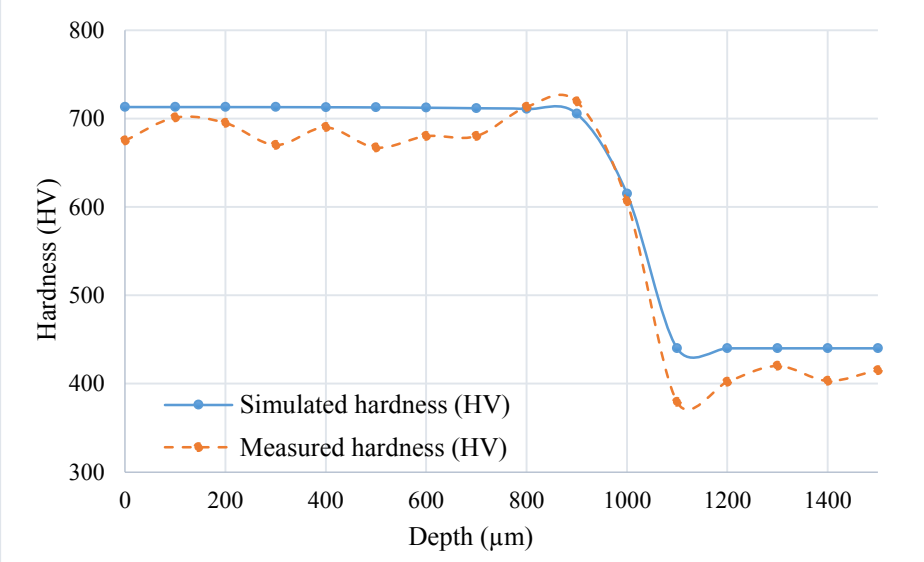

Figure 2.5 : Hardness curve for test 1 (850 W and 9 mm/s)

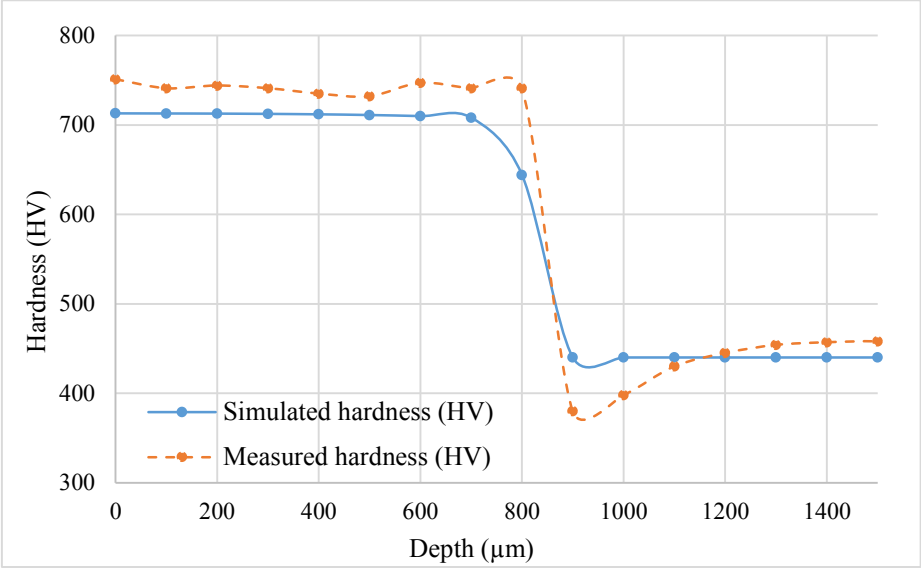

Figure 2.6 : Hardness curve for test 2 (850 W and 12 mm/s)

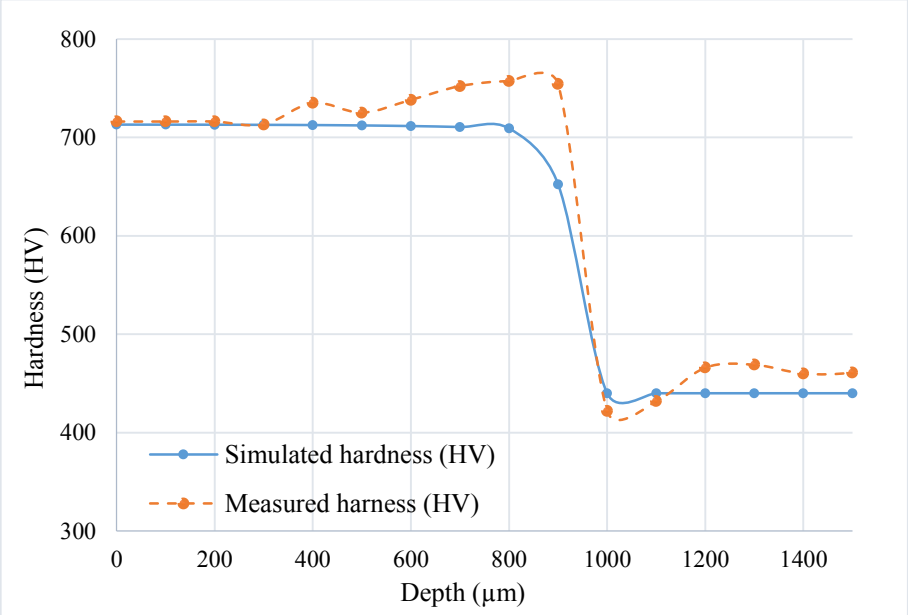

Figure 2.7 : Hardness curve for test 3 (950 W and 12 mm/s)

2.2.5-Calibration of the model with corrected Rc

The coefficient Rc can be estimated around 0.6 for steel [3]. However, this coefficient greatly varies according to the surface temperature. Moreover, the surface temperature depends on the process parameters. In order to correctly calibrate Rc, different combinations of process parameters are executed using laser heating cell and the Rc is corrected so the results generated by the simulation match the experimental results for each set of input parameters. Finally, Rc is approximated as a function of the process parameters using a linear regression technique. **Table 2.4** shows the Rc values depending on the laser power, the scanning velocity and the focus radius of the beam spot. The coefficient seems to increase as the power and/or the scanning velocity increases. Also, it seems to decrease when the focus radius increases.

Table 2.4 : Corrected Rc according to process parameters

Power P (W)	Scanning velocity V (mm/s)	Focus radius Rad (µm)	Corrected Rc
400	20	550	0.50
520	20	550	0.54
630	20	550	0.57
740	20	550	0.61
400	12	550	0.47
400	16	550	0.49
400	16	480	0.51
400	16	613	0.48
400	16	663	0.47

The regression equation (equation 11) proves that there is a linear relationship between Rc and the process parameters. The correlation coefficient is 0.994, which confirms a good correlation.

$$Rc=0.4205+0.000303\times P+0.003553\times V-0.000198\times Rad \quad (11)$$

P is the input power in W, V is the scanning velocity in mm/s, and Rad is the focus radius in µm. The developed equation is incorporated in the simulation model. The HD and HBW can be estimated with good accuracy as a function of the process parameters.

2.2.6-Shadowgraph measurements

As this study is focused on the HD and HBW and not the hardness values themselves, the depth and width are measured using optical method based on shadowgraph measurement. **Figure 2.8** shows a micrographic picture of a part heat treated by laser with a power of 1000 W and a scanning velocity of 12 mm/s. The hardened region with hard martensite appears very clearly after a chemical treatment and can even be observed with the naked eye. Two significant zones can be distinguished. The first one is the melted region near the surface that received a great amount of energy, enough to reach the melting point. The second region represents the hardened region where the temperature exceeded the austenitization temperature (Ac_3) without reaching the melting point and where the microstructure changed into martensite upon self-quenching.

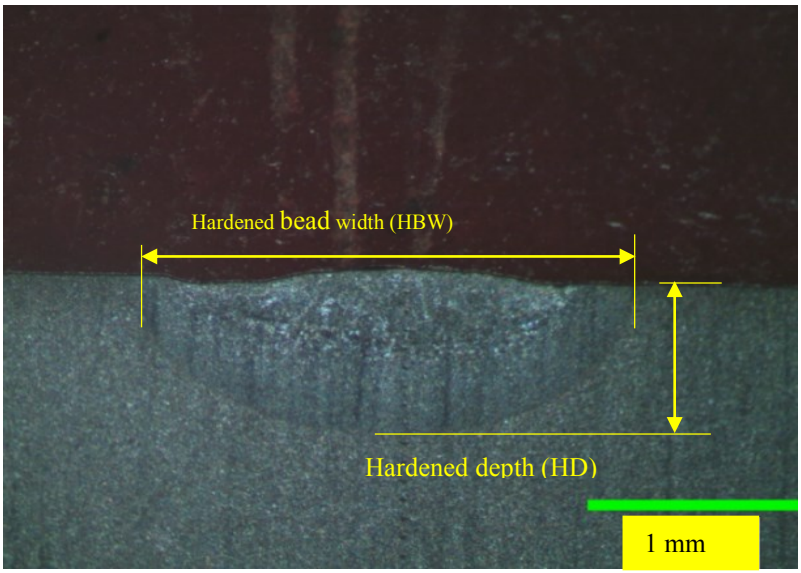

Figure 2.8 : Micrographic picture illustrating the HBW and HD after chemical etching

2.2.7-Statistical study

In the present study, the objective is to predict the HD and HBW with given process parameters provided by the great number of data generated through simulation (assuming

the input parameters are included in the range of study). A statistical study is conducted through a design of experiment (DOE) to determine the relative significance of each parameter and the interactions between them. The ANOVA method aims to study the effects of parameters on the hardness. It gives the contribution of each parameter on the variation of the outputs (HD and HBW). The process parameters and their design levels are displayed in **Table 2.5.** The levels are chosen so that the surface transformation happens and the surface temperature does not hit the melting temperature regardless of the combination of process parameters.

Table 2.5 : Factors and levels used for the ANOVA study

Factors	Factor Levels			
Laser Power (P) [W]	410	520	613	740
Scanning Velocity (V) [mm/s]	12	16	18	20
Focus Radius (Rad) [μm]	480	550	613	663

The simulation allowed us to quickly obtain results for all 64 (4^3) possible combinations of factor levels, and thus to generate a full factorial design. Statistical studies such as analysis of variance, main effects studies and linear regression are conducted.

2.2.7.1-Anova for HD versus P, V and Rad

Table 2.6 presents the detailed statistical analysis. An F-value above 11.77 implies that the parameter is very significant. In this case, power (P), scanning velocity (V), focus radius (Rad) are all significant models terms. The interaction terms are less important since their contributions are less than 0.4 %. Also, it is clear that the power and the scanning velocity have the largest effect on the response value and that they are equivalent with contributions around 48 %. The three interaction terms can be considered negligible.

Table 2.6 : ANOVA for HD

Source	DF	SS	contribution	MS	F-value	p-value
P	3	563906	48.4 %	187969	499.71	0.000
V	3	568906	48.8 %	189635	504.14	0.000
Rad	3	13281	1.1 %	4427	11.77	0.000
P×V	9	4531	0.4 %	503	1.34	0.264
P×Rad	9	2656	0.2 %	295	0.78	0.632
V×Rad	9	2656	0.2 %	295	0.78	0.632
Model	36	1155936	99.1 %	383124		
Error	27	10158	0.9 %	376		
Total	63	1166094				

Figure 2.9 shows the effect of all parameters on the case depth (HD). The obtained results confirm that the HD increases as beam power increases and/or as scanning velocity decreases. It also increases as the focus radius decreases. The ANOVA method is conducted in order to assess the significance of each parameter. For each parameter studied, the variance ratio value, F, is compared to the values from standard F-tables for given statistical levels of significance. In this way, it is concluded that within the investigated processing ranges, the power, the scanning velocity and the focus radius are significant for the case depth at 95 % confidence. Since the interaction terms have negligible contributions, they will not be considered in the rest of the study. **Figure 2.10** shows the HD calculated using the regression formula (equation 12) for all 64 combinations of process parameters and their distribution around the bisector of the quadrant. If the formula is perfectly accurate, all the points should be on the bisector. For the regression formula to be considered accurate, a maximum relative error of 10 % is allowed for all 64 sets of process parameters. A maximum relative error of 6.51 % is observed, with a mean relative error of 2.25 % between the HD calculated with the regression formula and the one simulated by the software. The coefficient of determination R^2 is mainly used to measure the relationship between experimental data and measured data. A coefficient $R^2 = 99.13$ % indicates an accurate study.

$$HD=1113.7+0.7557\times P-31.70\times V-0.2036\times Rad \quad (12)$$

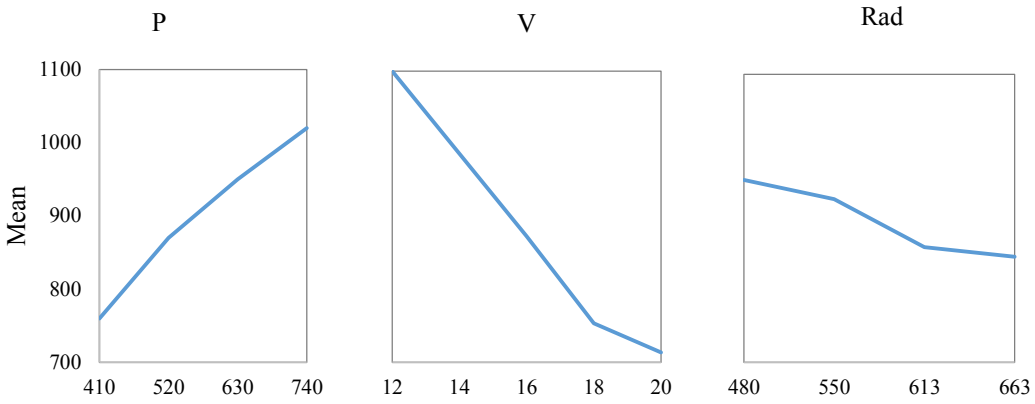

Figure 2.9 : Effects of parameters on case depth

2.2.7.2-Anova for HBW versus P, V and Rad

Table 2.7 shows the detailed statistical analysis. An F-value above 70.68 implies that the parameter is very significant. In this case, power (P), scanning velocity (V), focus radius (Rad) are all significant models terms. The interaction terms are less important since their contributions are less than 0.7 %. Also, it appears that the input power and the scanning velocity have the largest effect on the response value with contributions around 37-43 %. The three interaction terms can be considered negligible. The coefficient of determination R^2 is mainly used to measure the relationship between experimental data and measured data. Just like for the hardened depth, the input laser power and the scanning velocity have the same degree of impact (and the opposite effect); the other parameter (Rad) still have significance, and the interactions are negligible.

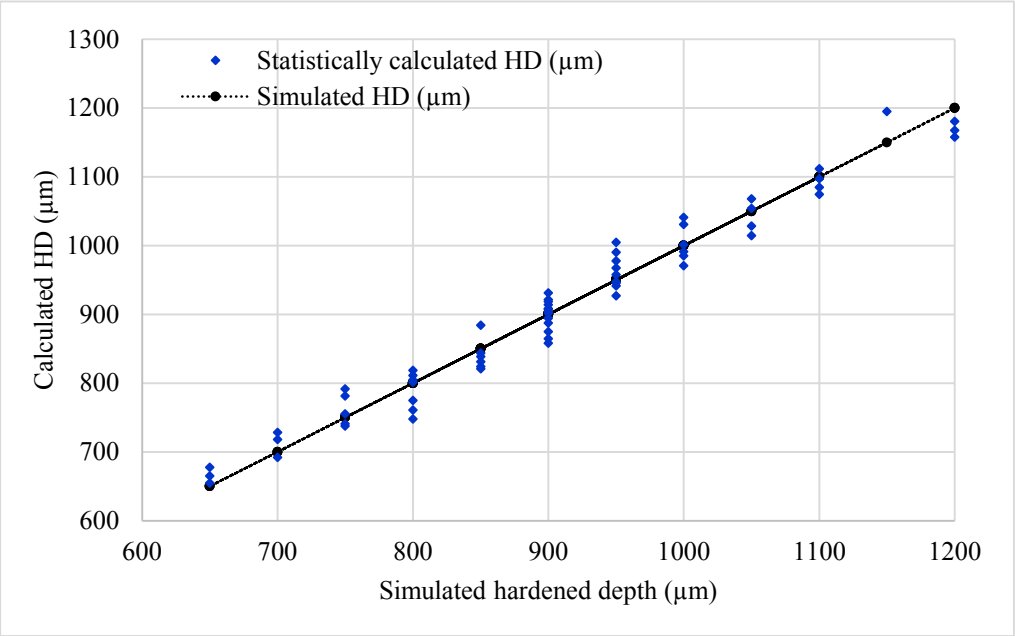

Figure 2.10 : Comparison between simulated HD and HD calculated by regression formula (equation 12)

Table 2.7 : Results of the ANOVA for HBW

Source	DF	SS	Contribution	MS	F-value	p-value
P	3	1763125	37.4 %	587708	161.71	0.000
V	3	2023125	43 %	674375	185.56	0.000
Rad	3	770625	16.4 %	256875	70.68	0.000
P×V	9	13125	0.3 %	1458	0.40	0.923
P×Rad	9	30625	0.7 %	3403	0.94	0.511
V×Rad	9	10625	0.2 %	1181	0.94	0.959
Model	36	4611250	98 %	1525000		
Error	27	98125	2 %	3634		
Total	63	4709375				

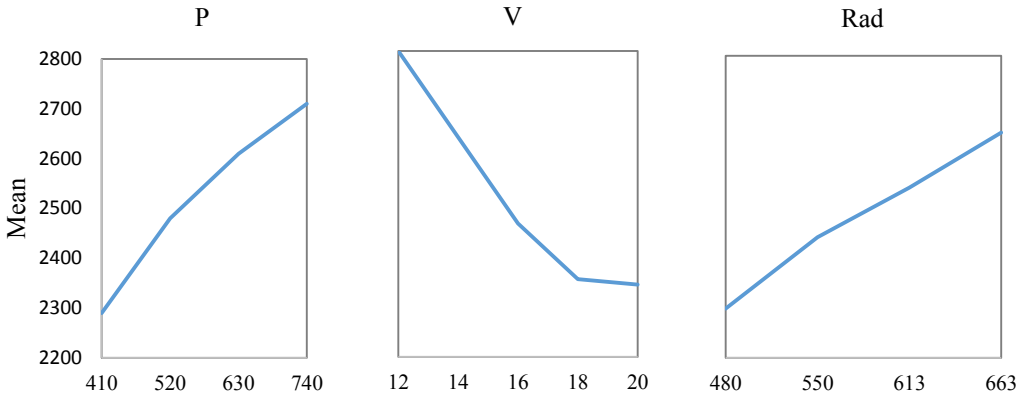

Figure 2.1 : Main effects plot for hardened bead width

The first thing one can notice on **Figure 2.11** is that the main effects plot for HBW is similar to the main effects plot for the HD, with the noticeable exception of the focus radius, which has the opposite effect on the HBW compared to the effect it has on the HD. Indeed, when the focus radius increases the HBW increases as well, whereas the HD decreases (see **Figures 2.9** and **Figure 2.11**). This is caused by the Gaussian distribution of the energy at the surface of the material, which results in a relationship between HD and HBW. Indeed, the fact that the radius is greater while the power and the scanning velocity remain the same means that there will be less energy at the center of the focus.

As for the HBW, it appears that the interactions are negligible with very low F-value. Therefore they will not be included in the regression equation.

Figure 2.12 shows the HBW calculated using the regression formula (equation 13) for all 64 combinations of process parameters and their distribution around the bisector of the quadrant. If the formula is perfectly accurate, all the points should be on the bisector. A maximum relative error of 6.95 % is observed, with a mean relative error of 2.39 % between the HBW calculated with the regression formula and the one simulated by the software. Both values are well under the maximum criteria of 10 % and thus, the formula can be considered accurate.

Moreover, the coefficient of determination R^2 = 97.92 % testifies an accurate regression equation albeit not as satisfying as it is for the HD.

$$HBW=1782+1.3409\times P-57.68\times V+1.598\times Rad \quad (13)$$

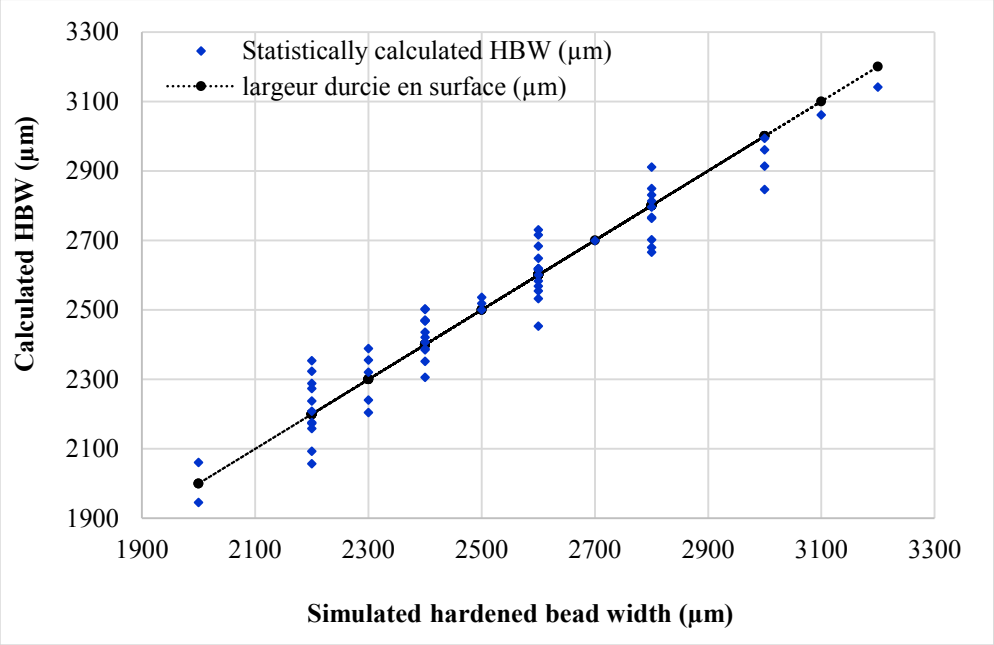

Figure 2.12 : Comparison between simulated HBW and HBW calculated by regression formula (equation 13)

In addition to the statistical study, and in order to provide a reliable alternative to standard thermal techniques that would be accurate and less time consuming, we conducted a study with an artificial neural network (ANN).

2.2.8- Neural network modeling

As compared to other techniques, an ANN provides a more effective modeling capability, particularly when the relationship between sensor-derived information and the characteristic(s) to be identified is non-linear. ANNs can handle strong non-linearity, a large number of variables, and missing information. Based on their intrinsic learning capabilities, ANNs can be used in a case where there is no exact knowledge concerning the

nature of the relationships between various variables. This is very useful in reducing experiment efforts.

A neural network is used to predict the hardened depth and hardened bead width. Neural networks are generally presented as systems of interconnected neurons, where the links between neurons are weighted. **Figure 2.13** shows the general principle of an ANN model. The goal is to produce one or more outputs that reflect the user-defined information stored in the connections during training.

In this study, a Generalized Feed-Forward Multilayer Perceptron (GFF-MLP) neural network model with one hidden layer containing 7 neurons is chosen. While various ANN techniques can be used in this approach, generalized feed forward networks seem to be the most appropriate because of their simplicity and flexibility. Before selecting the variables and training the models, it is important to establish the network topology and optimize the training performances. The idea is to approximate the relationship between the network parameters and the complexity of the variables to be estimated. The selected network is that which achieved the best results, the [n | 2n+1 | 3] network, where n is the number of inputs. The perceptron is characterized by a nonlinear sigmoid function. This type of neural network is always fully connected, meaning each perceptron of each layer is connected with all the perceptrons in the previous layer [31]. In a GFF-MLP network, connections between layers can jump over one or more layers. In practice, these networks solve problems much more efficiently than MLP networks [32].

Neural networks need to be trained with data sets in order to be able to interpolate for any given input parameters that fall within the training range. Neural networks cannot extrapolate, which means one cannot get reliable outputs if the input parameters are not within the range of the training parameters. In this study, the goal is to obtain a neural network able to predict the case depth and hardened bead width for a given combination of input parameters (within its training range). In all neural networks, during the training step,

the input data are normalized to the range of [-1, 1]. The weights and biases of the network are initialized to small random values to avoid a fast saturation of the activation function.

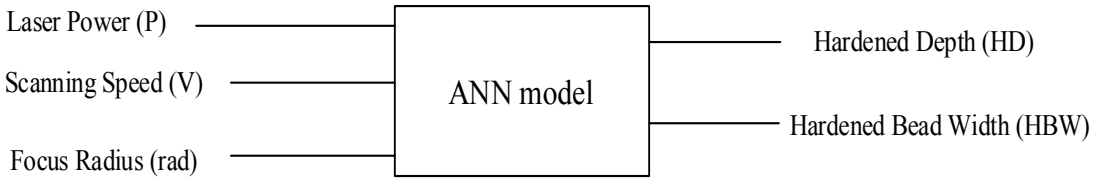

Figure 2.13 : Principle of the neural network

2.2.8.1-Maintaining the integrity of the specifications

For a commercial laser device, there are usually 3 control parameters, the input power (P), the scanning velocity (V) and the focus radius (Rad). In this study, 4 levels for each of those parameters are chosen and are displayed in **Table 2.5**. The levels are chosen to ensure minimal martensitic transformation and to avoid the melting point (about 1450°C) regardless of the combination of levels. With 3 parameters with 4 levels, the total number of possible combinations is 64 (4^3). The simulation allows to quickly get all of the 64 combinations and produce a full L64 matrix as in the preceding statistical studies.

In addition to the training data, a neural network also requires verification data (that are different from the training data) in order to validate the training step. These verification data are displayed in **Table 2.8**. In this case, the mean value of two consecutive levels are identified and used in simulation to generate data for verification. This leads to a validation design of 3^3 possible.

The neural network is trained considering the mean square error (MSE) of the cross-validation as an achievement indicator. The training of the neural network stops when the MSE stops decreasing. In order to evaluate the effectiveness of the network, some criteria are used, the correlation coefficient and the root mean square error, which would be respectively equal to 1 and 0 in the best case scenario with perfect accuracy.

Table 2.8 : Middle points

Factors	Factor Levels		
Laser Power (P) [W]	465	575	685
Scanning Velocity (V) [mm/s]	14	17	19
Focus Radius (Rad) [µm]	515	581.5	638

2.2.8.2-Result and interpretation

Once the training step of the network is performed, the 27 combinations of verification data are applied as input parameters. The outputs of the ANN model are compared with those obtained by simulation. Therefore, this comparison is effective using various statistical indexes that characterize the prediction capability of the ANN model. Two main criteria are used to evaluate the accuracy of the network: the absolute error and the relative error.

Figure 2.14 shows the absolute errors for both HD and HBW for all 27 test combinations. The maximum absolute errors for HD and HBW are, respectively, 64 and 94 µm. This means that the absolute error is of less than 100 µm for the overall test data, for both HD and HBW. Given that the values of HD are between 700 µm and 1100 µm, and that the values of HBW are between 2400 µm and 3000 µm, the model exhibits a good potential in terms of accuracy.

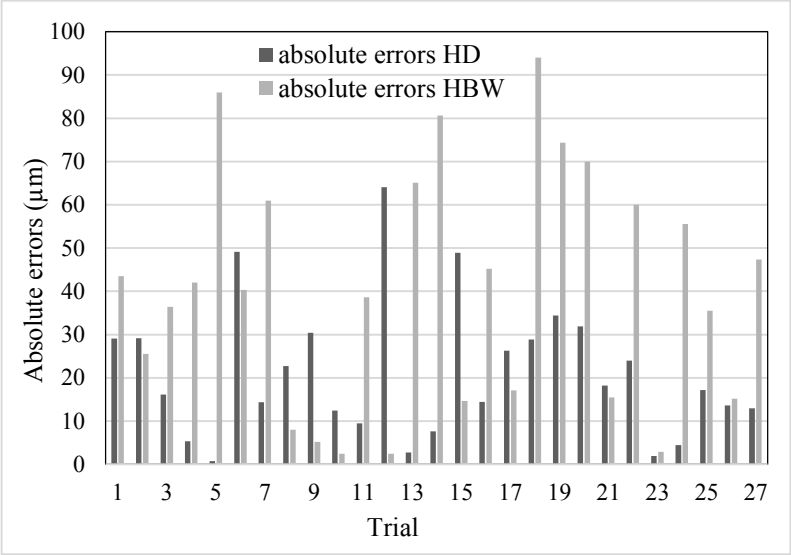

Figure 2.14 : Absolute relative errors for HD and HBW

As can be seen in the **Figure 2.15**, the relative errors for both the HD and HBW are very low in every case. The maximum relative errors for HD and HBW are, respectively, 8.01 % and 3.62 %. The mean relative errors for HD and HBW are 2.40 % and 1.63 %, respectively, which heightens the accuracy of the neural network.

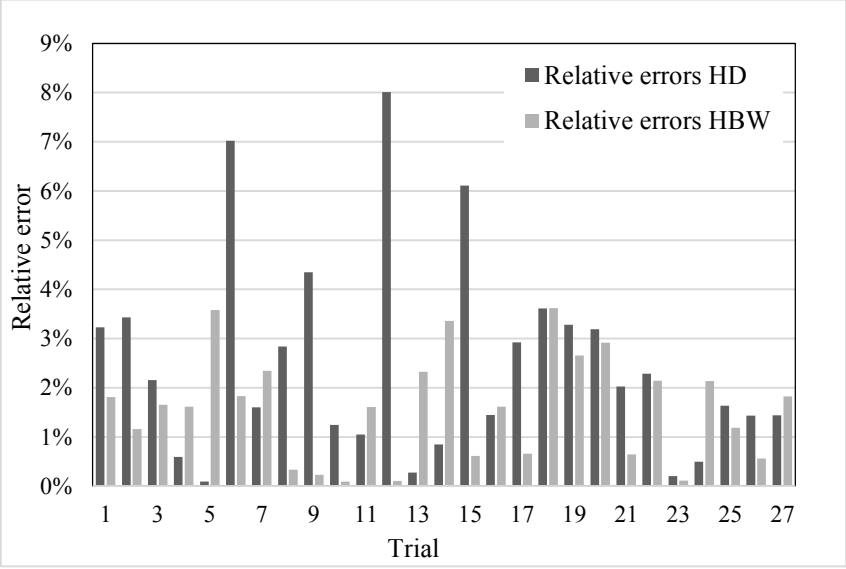

Figure 2.15 : Relative errors for HD and HBW

Figures 2.16 and **Figure 2.17** present, respectively, the results of the ANN models during the verification stage for HD and HBW. In fact, the figures show the ANN model and those obtained by simulation. The data are mostly located around the bisector of the 1st quadrant, which outlines the accuracy of the model. The two figures show that the network is well trained and is highly efficient. The network is therefore a reliable way to predict the HD and HBW for any combination of input parameters within the training range (between 480 W and 663 W for power, 12 mm/s and 20 mm/s for scanning velocity, 480 mm and 663 mm for focus radius). The ANN models don't require any computation time to predict the outputs comparatively to the simulation. Note that the ANN models can predict the desired outputs in the studied variation range only and they cannot extrapolate outside.

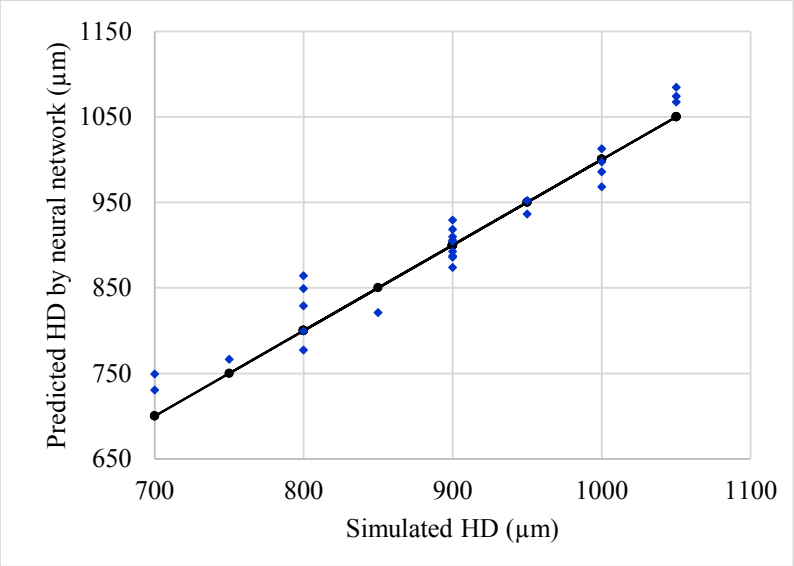

Figure 2.16 : Comparison between simulated HD and HD calculated by the neural network.

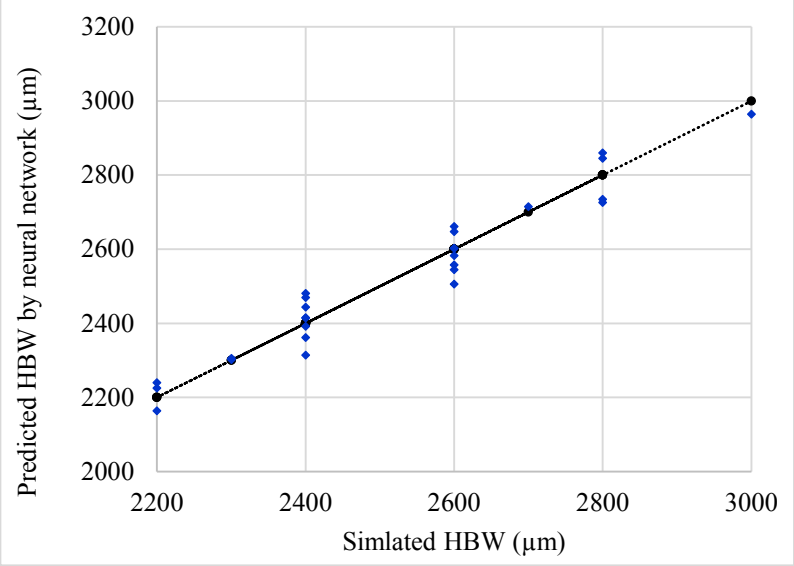

Figure 2.17 : Comparison between simulated HBW and HBW calculated by the neural network

Table 2.9 shows the comparison between the results generated by simulation and those generated by ANN model during training stage and confirms the observations from **Figure 2.14** and **Figure 2.15**.

Table 2.9 : Comparison of the results

		Simulation		ANN models		Absolute error		Relative error	
		HD (µm)	HBW (µm)	HD (µm)	HBW (µm)	HD (µm)	HBW (µm)	HD (%)	HBW (%)
Training	Min	700	2000	698	2058	2	58	0.03	0.05
	Max	1200	3200	1175	3147	25	53	4.88	4.52
	Mean	937	2557	931	2570	15	39	1.62	1.55
Verification	Min	700	2200	730	2164	1	2	0.10	0.09
	Max	1050	3000	1084	2964	64	94	8.01	3.62
	Mean	894	2522	902	2521	21	40	2.40	1.63

Even if the ANN models have good performances in terms of robustness and accuracy, it is still important to validate them using experimental validation.

2.2.9-Experimental validation of the neural network

The great number of data that can be generated by a 3D finite element simulation allows to accurately train a neural network that will be able to predict the HD and HBW, and thus, it avoids the need to produce expensive experimental data that are often less numerous because of their cost.

Once the network accuracy is verified with data generated by a FEM simulation, experimental validation tests are conducted using a Nd:Yag laser and the shadowgraph measurement method.

Eight sets are randomly chosen among the 27 sets of verification data. The experimental matrix is displayed in **Table 2.10**.

The input powers are between 465 W and 685 W, the scanning velocities are between 14 mm/s and 17 mm/s. Finally, the focus radii are between 515 µm and 638 µm.

Table 2.10 : Experimental matrix for validation

Test	Power (W)	Scanning velocity (mm/s)	focus radius (µm)
1	465	14	515
2	575	19	515
3	685	17	515
4	685	14	515
5	575	14	581.5
6	685	17	581.5
7	465	17	638
8	685	17	638

The results of the tests are shown in **Table 2.11**. The maximum relative errors for both the HD and HBW are 7.37 % and 2.93 %, respectively.

The ANN is able to correctly predict both HD and HDW. It can now be used independently from the COMSOL software. It is easier to use as one only needs to compute

the process parameters (within the training ranges of the ANN) to obtain reliable results instantly.

Table 2.11 : Experimental validation – results

Test	Network HD (µm)	Experimental HD (µm)	Relative error for HD (%)	Network HBW (µm)	Experimental HBW (µm)	Relative error for HBW (%)
1	929	909	2.2	2444	2375	2.88
2	864	894	3.35	2302	2320	0.76
3	968	953	1.59	2470	2402	2.83
4	1084	1010	7.37	2726	2653	2.74
5	997	1018	2.04	2735	2702	1.22
6	952	1022	6.86	2603	2591	0.46
7	777	785	0.98	2392	2324	2.93
8	936	1002	6.55	2715	2643	2.73

2.2.10-Conclusion

In this paper, a structured and comprehensive approach developed to design an effective ANN-based model for quality assessment and prediction in LSTHP using a commercial 3 kW Nd:Yag laser is presented. Several laser hardening parameters and conditions were analyzed and their correlation with multiple performance characteristics of hardened surface was investigated using a structured experimental investigations and exhaustive 3D FEM simulations under consistent practical process conditions. Following the identification of the hardening parameters and conditions that provide the best information about the LSTHP operation, tow type of modeling techniques were proposed to assess and predict the hardened bead width and hardened depth (HD) of the laser transformation hardened AISI 4340 steel plate: multiple regression analysis and ANN approach. The results demonstrate that the regression approach can be used to achieve a relatively accurate predicting model with correlation larger than 90 %. The ANN models present greater results. The maximum relative errors for both HD and HBW are less than 8 % and 3 %, respectively. Globally, the performance of the ANN-based model for quality estimation and prediction in LSTHP shows significant improvement as compared to conventional methods. With a global maximum relative error less than 10 % under various

LSTHP conditions, the modeling procedure can be considered efficient and have led to conclusive results, due to the complexity of the analyzed process. The proposed approach can be effectively and gainfully applied to quality assessment for LSTHP, because it includes the advantages of ease of application, reduced modeling time and sufficient modeling accuracy.

CHAPITRE 3
ANALYSE THERMIQUE DU TRAITEMENT SURFACIQUE AU LASER DES ENGRENAGES-SIMULATION 3D ET VALIDATION

3.1-RESUME EN FRANÇAIS DU TROISIEME ARTICLE

L'article aborde le cas de la simulation numérique du procédé de traitement thermique superficiel au laser dans le cas d'une géométrie complexe (ici des dents d'engrenage). Les résultats, qui sont la profondeur durcie au sommet et au pied des dents, donnés par la simulation sont ensuite vérifiés par des essais expérimentaux. L'engrenage est monté sur un tour en rotation et le faisceau laser balaye ensuite l'engrenage sur toute sa largeur. Le modèle numérique simule ce traitement avec un flux de chaleur à travers la surface du matériau auquel on impose un mouvement de rotation et de translation. Il est vite apparu qu'un préchauffage avec de rapides balayages laser en va-et-vient à faible puissance est nécessaire pour amener la température des dents proche de la température d'austénitisation. Un unique balayage final à forte puissance permet alors de traiter les dents en profondeur. Les profils de traitement obtenus par la simulation et la validation expérimentale sont très similaires à ceux obtenus par le procédé de traitement par induction couramment utilisé dans l'industrie de nos jours pour le traitement des dents d'engrenages.

Ce troisième article, intitulé « *Thermal analysis of surface transformation hardening of gears using laser – 3D simulation and validation* », fut corédigé par moi-même ainsi que par les professeurs Abderrazak El Ouafi et Noureddine Barka, respectivement second et troisième auteur. En tant que premier auteur, ma contribution à ce travail fut l'essentiel de la recherche sur l'état de l'art, le développement de la méthode, l'exécution des tests de performance et la rédaction de l'article. Les professeurs Abderrazak

El Ouafi et Noureddine Barka ont fourni l'idée originale. Ils ont aidé à la recherche sur l'état de l'art, au développement de la méthode ainsi qu'à la révision de l'article.

3.2- THERMAL ANALYSIS OF SURFACE TRANSFORMATION HARDENING OF GEARS USING LASER – 3D SIMULATION AND VALIDATION

G. Billaud
Mathematics, Computer Science and Engineering Department
University of Quebec at Rimouski
Rimouski, Canada, G5L 3A1

A. El Ouafi
Mathematics, Computer Science and Engineering Department
University of Quebec at Rimouski
Rimouski, Canada, G5L 3A1

N. Barka
Mathematics, Computer and Engineering Department
University of Quebec at Rimouski
Rimouski, Canada, G5L 3A1

3.2.1-Abstract

This paper presents the study of the laser surface transformation hardening of a low alloy AISI 4340 steel workpiece of finite width such as a gear. A 3D model implemented on a commercial software enables solving the heat transfer equation, the determination of the temperature distribution under the surface as well as the prediction of optimal process parameters. The laser beam is considered as a moving disc heat flux through the surface, with a Gaussian distribution of heat intensity. With a temperature distribution that can be determined at any given time during the process, the width and depth of the hardened zone beneath the surface can be determined using the Ashby and Easterling metallurgical equations.The process parameters are the laser power, P, the laser beam focus diameter, D_{foc} , and the traverse scanning velocity, V_{sc}. In this study the gears are mounted on a lathe, and the laser beam is immobile and placed above the rotating gear. This adds another control parameter, rotation speed, W_r. A commercial Nd:Yag laser beam is used to validate the simulated results. The results demonstrate that the numerical simulation can effectively lead to a consistent model able to accurately and reliably provide an appropriate prediction of hardened surface characteristics of gear teeth under variable hardening parameters, without requiring an actual expansive trial and error procedure. In addition, the

results of the experimental procedure conducted in this study appears to be very comparable with those obtained by the induction process.

Keywords: Laser transformation hardening process, Nd:YAG laser, Hardened depth, Hardened bead width, gears.

3.2.2 -Introduction

The type of microstructure under the surface that forms during manufacturing affects the fatigue performance of mechanical components. The wear resistance of steel components, such as gears or bearings, depends on their surface hardness [33]. Different types of surface hardening processes are used to achieve the required hardness, such as induction hardening or case carburization. Another method is to use a laser beam. Lasers are becoming more and more widely used in industrial applications including cutting, drilling, welding and heat treatment (among many others) [2]. The laser hardening process, which is the subject of the present study, can be fully computer-controlled or numerically controlled. In the case of steel components with complex geometries such as gears, a laser beam allows a very localized and selective hardening with control of treated depth and width [2]. Moreover, the localized heating reduces the thermal distortions to a minimum. The rapid heating allows the transformation of the steel into austenite before it is transformed into hard martensite upon cooling, due to rapid heat conduction into the colder core of the steel (self-quenching). Surface melting is to be avoided in laser surface hardening of steels. With the melting temperature of low alloy steels like AISI 4340 being around 1430 °C, it limits either the maximum power density (which depends on the laser power and the beam focus diameter) or the minimum scanning velocity. Nevertheless, the power density must be high enough and the interaction time must be long enough for the steel to transform from its initial microstructure into austenite. This sets either the minimum power density or the maximum scanning velocity. For AISI 4340 the transition temperature from the initial microstructure to complete austenite is at about 800 °C. In the case of laser surface transformation, the cooling rate is generally above 10^3 °C/s, which is more than enough for the martensite to be produced in most low alloy steels, including

AISI 4340 steel. The main process parameters are generally the laser power, scanning velocity and beam diameter. Optimizing and reducing the laser heat treatment cost is an issue in aerospace and automotive industries. Because experimentation is expensive in the case of laser heating, it is better to be able to predict the results of laser heat treatment depending on the parameters.

3.2.3-Literature review

Steen and Courtney [34] conducted a study of the laser transformation of AISI 1036 steel using a 2 kW continuous wave CO2 laser. A five level, full factorial design experiment was conducted with power levels from 1.2 kW to 2 kW, scanning velocities from 25 mm/s to 400 mm/s, and beam radii from 1.6 mm to 5.8 mm. With these experiment designs, they statistically established a relationship between the hardened depths and the process parameters.

Ashby and Easterling [5] conducted a study of the transformation hardening of hypo-eutectoid steels using a laser beam. They used 500 W and 2500 W continuous CO2 lasers with both Gaussian and “top hat” energy profiles. They combined approximate solutions for the heat flow with kinetic models to predict the change of microstructure and hardness with depth. Finally, they produced diagrams which showed the beam power density, beam radius, scanning velocity, depth below the surface for a given microstructure, and the resulting hardness profiles.

Following the work of Ashby and Easterling, Davis et al. [13] included kinetic models describing the change of microstructure in their thermal analysis of a rectangular workpiece.

Steen and Mazumder [3] established a three dimensional heat transfer model for laser material processing, with a moving Gaussian distribution heat source, by using finite difference numerical techniques. In their study, they considered the system to be in quasi-steady-state conditions, in that the thermal profile was considered to be steady relative to the position of the laser beam.

Generally, the thermal properties of carbon steels, such as thermal conductivity and specific heat, as well as the surface absorptivity, are strongly dependant on temperature. Only one value of those properties can be used in an analytical method. Kou et al. [35] addressed the issue of thermal properties varying depending on temperature. They conducted a theoretical and experimental study of heat-flow and solid-state phase transformations during the laser surface hardening of 1018 steel with a continuous wave CO2 laser of 15 kW capacity. They established a three dimensional model using the finite difference method that takes into account the temperature dependence of the thermal properties.

Patwa and Shin [17] conducted an accurate study on the modeling of the laser hardening process of laser operating parameters and initial microstructure without the need for experimental data. Their model combined a three dimensional transient numerical solution for an AISI 5150H steel rotating cylinder mounted on a computer-numerically controlled lathe. They used a kinetic model to determine the phase change using the CCT diagram of the steel. Their model was able to accurately predict the case depth as well as the hardness.

Concerning complex geometries such as gears, an analytical study of the laser surface transformation hardening process was conducted by R. Komanduri and Z.B. Hou [36] to determine the temperature distribution generated by a laser heat source (and thus the depth and width of the case hardening) depending on the process parameters. They made a comparative study between their analytical approach and the semi-empirical relationships developed by Steen and Courtney [34]. Some years later, R. Komanduri and Z.B. Hou [37] used their established analytical model to optimize the process parameters for different heat intensity distributions, such as normal (pseudo-Gaussian), uniform, or bimodal (TEM11), that allow more uniform case hardening depth than the Gaussian distribution (TEM00). Their study established the theoretical optimized ranges of power and scanning velocity depending on the heat intensity distribution and the laser beam diameter.

An interesting study was conducted by H. Zhang [9] et al. that compared the contact fatigue strength of carbon case hardening and laser hardening of gear teeth. The carbon case hardening has the shortcoming of generating very large distortions necessitating regrinding. The laser hardening process does not have this inconvenience. According to their study, the contact fatigue strength limit of laser hardened gears was found to be 92 % that of those treated by carbon case hardening.

The objective of this paper is to present the simulation of the laser surface transformation in the case of complex geometries, such as gears, which are rarely treated in the literature. It is an extension of the study conducted by G. Billaud et al [38].The aim is to develop a method that enables predicting the results of gear treatment without conducting expensive physical experiments. The simulation is validated by experimental tests using a test bench made for that purpose. The gears are made of a commonly used AISI 4340 low alloy steel that is well known in industry for its good hardenability. The proposed approach examines laser hardening parameters commonly known to influence the characteristics of hardened surfaces, such as input power, scanning velocity and focus radius. However, the process presented in this study involves a rotational movement of the gear, so an additional parameter, the rotation speed, is also taken into account.

3.2.4-Model description

One issue with the laser surface transformation of a rotating workpiece with a lateral scanning velocity is that the uniformity of treatment is not guaranteed. Indeed, as shown in **Figure 3.1,** points A and B, which are diametrically opposed, are not heated by the laser in the same way.

In practice, in the case of gears, it would mean that two teeth diametrically opposed would not be heated and treated the same way. To avoid this problem, it is best to have a great rotation speed and a slow scanning velocity. However, if the scanning velocity is too slow, there is a risk that the surface temperatures may reach the melting temperature of the steel, which is undesirable. On the other hand, if the rotation speed is too high, the gear

teeth might not be heated enough to create a proper case depth. A compromise must therefore be found between these two parameters.

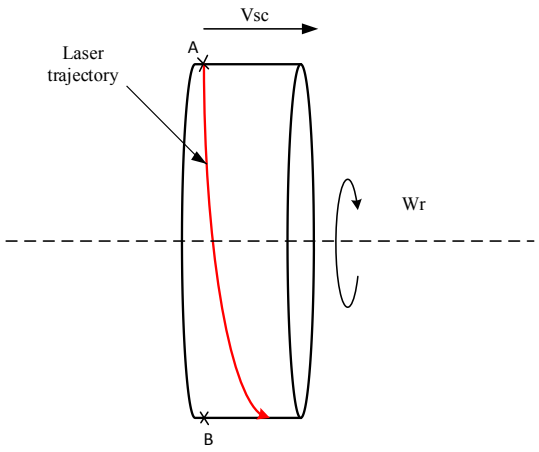

Figure 3.1 : Laser trajectory

In this study, the gear is made of AISI 4340 low alloy steel with 48 teeth. The gear has an external diameter of 105 mm (from the top of a tooth to the top of the opposite tooth), an internal diameter of 30 mm, and a width of 7 mm. In order to simulate the heating process using the finite element method, the part was built on a computer aided design software.

The gear is mounted on a shaft and clamped by two mounting rings on each side, as shown in **Figure 3.2**.

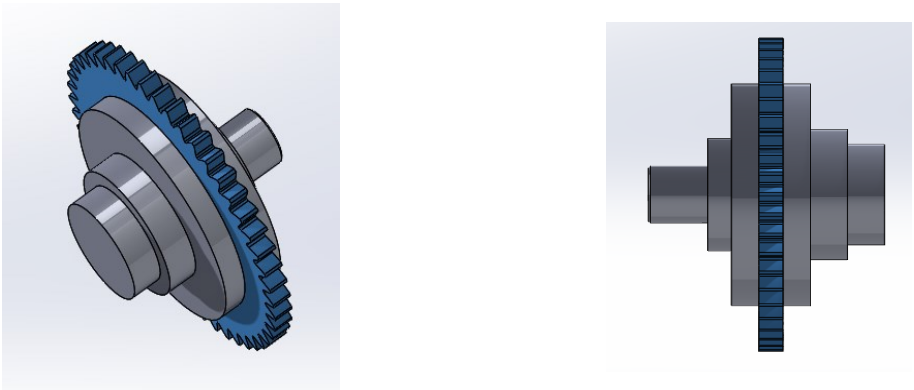

Figure 3.2 : The gear mounted on the shaft and clamped by two mounting rings

3.2.4.1-Heat equation

In this study, the heat flux used for the simulation was considered as a Gaussian type beam distribution, which is given by equation 1 [2].

$$\mathrm{E} = \mathrm{E}_0 \times \exp\{-2 \times [(\mathrm{y} - (y_0 + V_{sc} \times t))^2 + \alpha^2] / {D_{foc}}^2\} \quad (1)$$

E_0 and α are given by equation 2 and 3.

$$E_0 = 2 \times \mathrm{P} \times (1 - \mathrm{Rc}) / (\pi \times {D_{foc}}^2) \quad (2)$$

$$\alpha = \sin(w_r \times t) \times z - \cos(w_r \times t) \times x \quad (3)$$

D_{foc} is the Gaussian beam diameter, P is the laser beam power, $\mathrm{R_c}$ is the reflection coefficient of the surface of the chosen material [3]. V_{sc} is the scanning velocity, y_0 is the beam center coordinate along the y-axis at t = 0 s. E (in W/m2) represents a Gaussian heat flux moving along the y-axis with a velocity V_{sc} and simultaneously rotating around that axis with a rotation speed w_r.

Finally, α is orthonormal to the laser beam direction at the surface of the workpiece.

Table 3.1: Material properties

Property	Symbol	Unit	Value
Reflection coefficient	Rc		0.6
Eutectoid temperature	Ac_1	K	996
Austenitization temperature	Ac_3	K	1053
Austenite grain size (assumed)	g	μm	10
Activation energy of carbon diffusion in ferrite	Q	kJ/mol	80
Pre-exponential for diffusion of carbon	D_0	m^2/s	$6x10^{-5}$
Gas constant	R	J/mol.K	8.314
Steel carbon content	C		0.43 %
Austenite carbon content	C_e		0.8 %
Ferrite carbon content	C_f		0.01 %
Critical value of carbon content	C_c		0.05 %
Volume fraction of pearlite colonies	f_i		0.5375

As will be shown later in this study, the process requires a preheating of the gear teeth in order to create a decent, rather uniform, case depth. Therefore, in this study, T_0 will be the initial temperature of the gear teeth, and that temperature will be the chosen preheating temperature. The preheating experimental procedure is explained later in the paper.

Figure 3.3 shows the isothermal contours (zoomed in on few teeth) for a power of 2500 W, a scanning velocity of 1 mm/s and a rotation speed of 240 rpm. The preheating temperature (initial temperature) T_0 is set at 873 K.

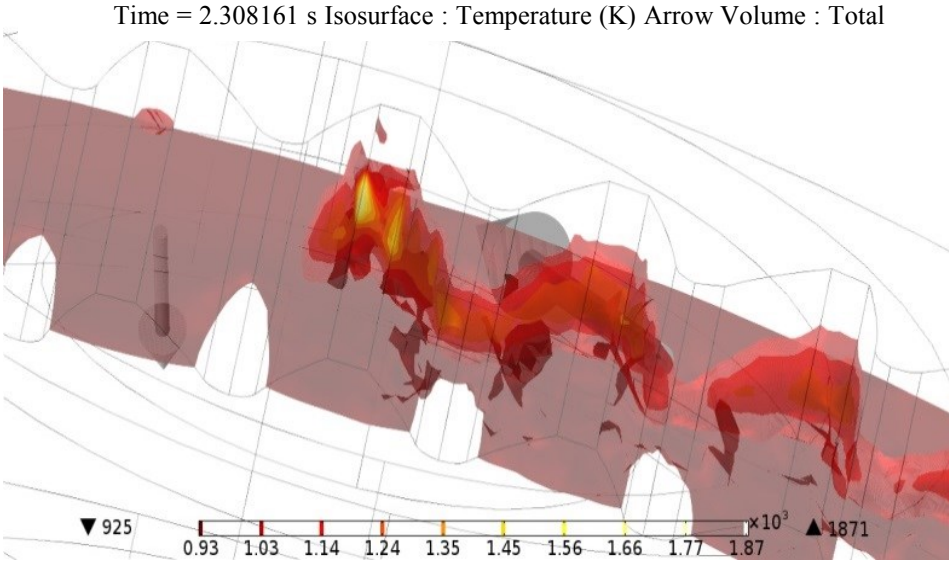

Figure 3.3 : Isothermal contours for P = 2500 W, V_{sc} = 1 mm/s, w_r = 240 rpm, T_0 = 873 K

Figure 3.3 shows that the temperature is at its maximum at the location of the laser, and greatly decreases both with the depth and after the laser has passed. The rapid decrease of temperature is essential for quenching of the steel to occur. However, in this figure, it can be seen that the surface temperature is too high (about 1871 K), and above the melting temperature of AISI 4340 steel (about 1450 K). An experiment under these conditions would most likely lead to a partial melting of the gear teeth, which is not desirable. It is worth noting that there is a heat concentration at the top of the teeth since the gear has sharp

corners. Concentrating the heat at such points could cause slight melting that would bow them during heat treatment.

Figure 3.4, Figure 3.5 and Figure 3.6 show the isothermal contours resulting from the simulation using the same laser power and scanning velocity at the same time step, but with different rotation speeds and a lower preheating temperature of 500 K. The figures show that the rotation plays a major role in the uniformity of the treatment. High rotation speeds greatly reduce the peak temperature (providing the other control parameters remain the same). At 60 rpm, the temperature increases to 1560 K (at t = 2.306089 s). At 120 rpm it increases to 1448 K at the same time step, while at 300 rpm it only increases to 957 K, which is not enough to achieve a proper case depth. Indeed, in the last case the peak temperature is under the austenitization temperature.

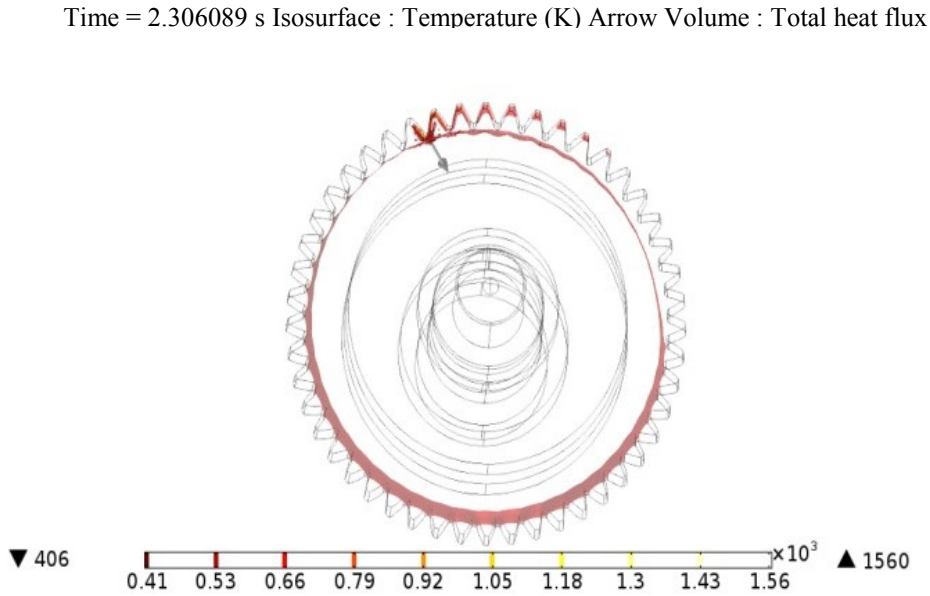

Figure 3.4 : Isothermal contours for P = 1500 W, V_{sc} = 1 mm/s, w_r = 60 rpm, T_0 = 500 K

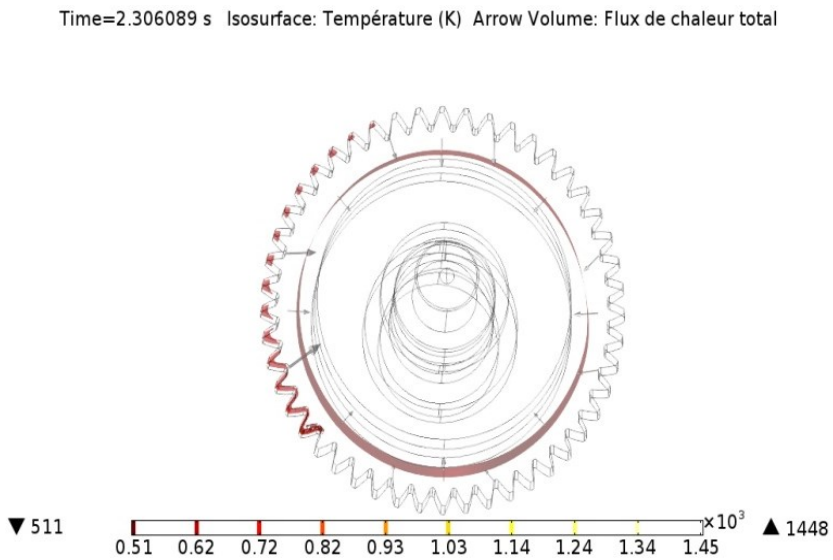

Figure 3.5 : Isothermal contours for P = 1500 W, V_{sc} = 1 mm/s, w_r = 120 rpm, T_0 = 500 K

Time = 2.306089 s Isosurface: Temperature (K) Arrow Volume : Total heat flux

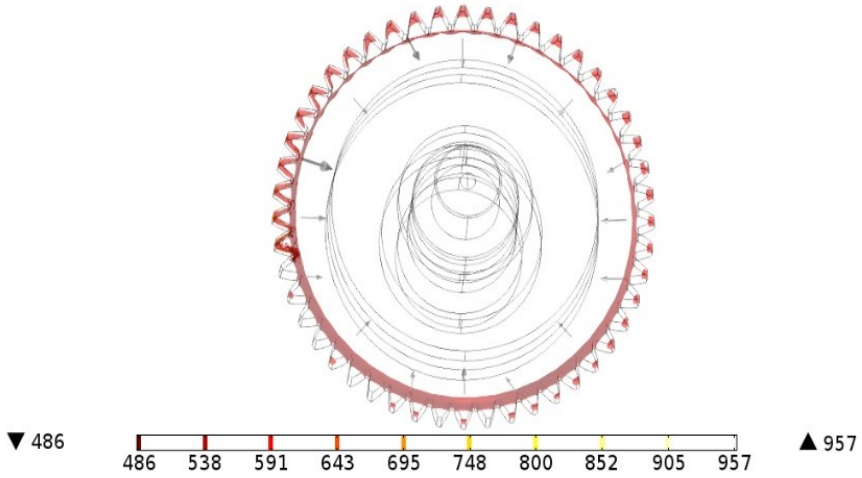

Figure 3.6 : Isothermal contours for P = 1500 W, V_{sc} = 1 mm/s, w_r = 300 rpm, T_0 = 500 K

3.2.4.2-Metallurgical equations

Once the temperature distribution is generated by the software, the temperature data can be extracted to determine the metallurgical transformations that occur during the surface transformation. The following metallurgical equations for a low alloy steel, established by Ashby and Easterling [5] are used to calculate the case depth.

The total number of diffusive jumps which occurs during the heat cycle affects the extent of the structural change and is given by the kinetic strength [5].

$$I = \int \exp\left\{-Q/\left(R \times T[t]\right)\right\} dt \tag{4}$$

Q is the activation energy for the transformation and R is the gas constant. The kinetic strength can also be simply expressed as in equation 5.

$$I = \alpha \times \tau \times \exp\left\{-Q/\left(R \times T_p\right)\right\} \tag{5}$$

Tp is the peak temperature at the considered depth and τ is the thermal time constant. The term α and τ are approximated by the equations 6 and 7.

$$\alpha = 3\sqrt{\left[\left(R \times T_p\right)/Q\right]} \tag{6}$$

$$\tau = \left(1\text{-}Rc\right) \times P/\left(2 \times \pi \times K \times e^1 \times V \times \left[T_p\text{-}T_0\right]\right) \tag{7}$$

T_0 represents the initial preheating temperature.

The obtained austenite has the same carbon content as a perlite microstructure c_e = 0.8 %. From there, the carbon diffuses in the proeutectoid ferrite. When the temperature reaches the austenitization temperature (about 1000 K), the volume fraction of austenite is the volume fraction f_i (which is also the minimum volume fraction of martensite).

$$f_i = \left(C\text{-}C_f\right)/\left(0.8\text{-}C_f\right) \approx C/0.8 \tag{8}$$

c_f is the negligible carbon content of the ferrite and c is the carbon content of the steel.

The maximum martensite fraction allowed by the transformation temperature time diagram (TTT diagram) is

$$\begin{aligned} fm &= 0 && \text{if } T_p < Ac_1 \\ fm &= fi+(1-f_i)\times(T_p-Ac_1)/(Ac_3-Ac_1) && \text{if } Ac_1 \le T_p \le Ac_3 \\ fm &= 1 && \text{if } T_p > Ac_3 \end{aligned} \quad (9)$$

Ac_1 is the austenitization temperature (the start of the transformation). Ac_3 (about 1073 K) is the temperature of complete austenitization (**Table 3.1**).

Ashby and Easterling supposed that all the material with a specific carbon proportion above a critical value, C_c, will transform into martensite. The volume fraction of the martensite is then given by equation 10 [2, 5].

$$f = fm-(fm-f_i)\times\exp\left\{-(12\times f_i^{2/3})/(g\times\sqrt{\pi})\times\ln\left[C_e/(2\times C_c)\right]\sqrt{(D_0\times I)}\right\} \quad (10)$$

g is the mean grain size and D_0 is the diffusion constant for the carbon in ferrite.

The hardness can then be calculated by a mixture rule (equation 11).

$$H=f\times H_m+(1-f)\times H_{f+p} \quad (11)$$

The values H_m and H_{f+p} are given by Maynier equations that take into account the cooling rate and the composition [21].

3.2.5-Experimental validation

3.2.5.1-Experimental setup

The experimental validation is performed by using a commercial 3 kW Nd: Yag laser (IPG YLS-3000-ST2), combined with an articulated robot with 6 degrees of freedom

(**Figure 3.7**). This type of laser generates a beam with a wavelength $\lambda = 1064$ µm. The gear is mounted on a lathe protected by a casing. The protective casing is fixed on a table and is placed under the laser head. The process parameters are the input power, the scanning velocity and the lathe's rotation speed. In this study, the laser beam has a continuous straight-line trajectory back and forth.

Figure 3.7 shows the complete experimental setup with the protective casing closed, the laser head above and ready to fire, and a thermal camera in the foreground to monitor the rising temperature.

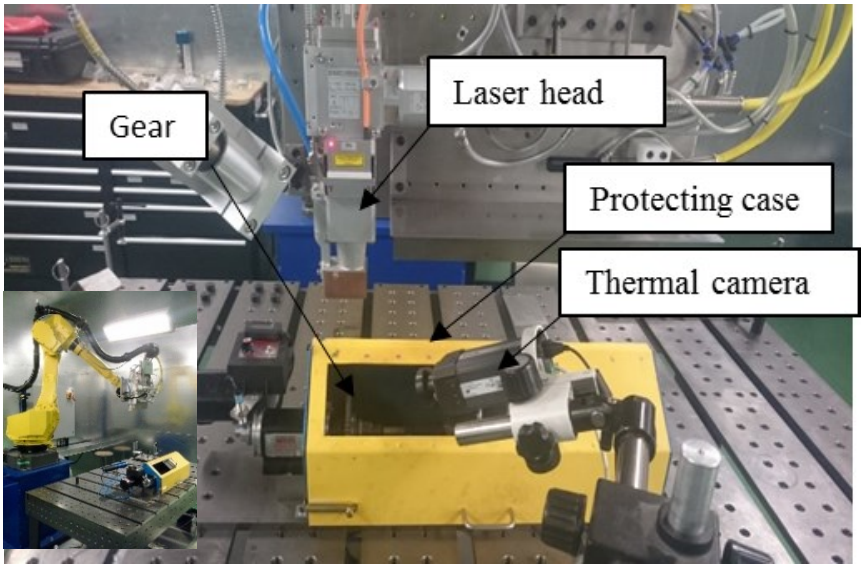

Figure 3.7 : Experimental Setup.

3.2.5.2-Preheating step

The preheating procedure consists of a series of very high speed laser sweeps back and forth in a short time and at moderately low power while the gear mounted on lathe is rotating.

A thermal camera indicates the temperature in the gear teeth in real time. The selected power for the preheating procedure depends on the desired preheating temperature.

However, the duration of the preheating treatment, which depends on the number of sweeps and their velocity, is always kept the same.

3.2.5.3-Heating treatment

Immediately after the preheating process, a surface transformation is performed by a single low speed laser scanning along the width of the gear at a high power. The gear is still rotating at the same speed during that step. The gear teeth quench themselves by rapid heat conduction into the colder core of the gear. The mounting rings and the shaft are heat conductors that facilitate rapid cooling.

3.2.5.4-Experimental tests and discussion

With the help of the simulation, a series of experimental tests was conducted in order to determine the effect of each parameter on the case depth at the top, the bottom and on the slope of the gear teeth, along the entire width of the gears.

Figure 3.8 and **Figure 3.9** show the treatment for two different scanning velocities (the other process parameters and the preheating procedure remain the same). The small treated zone appears darken under the surface of the tooth at the top, the bottom and on the slope of the tooth. The core of the material (in bright) remained unaffected by the treatment.

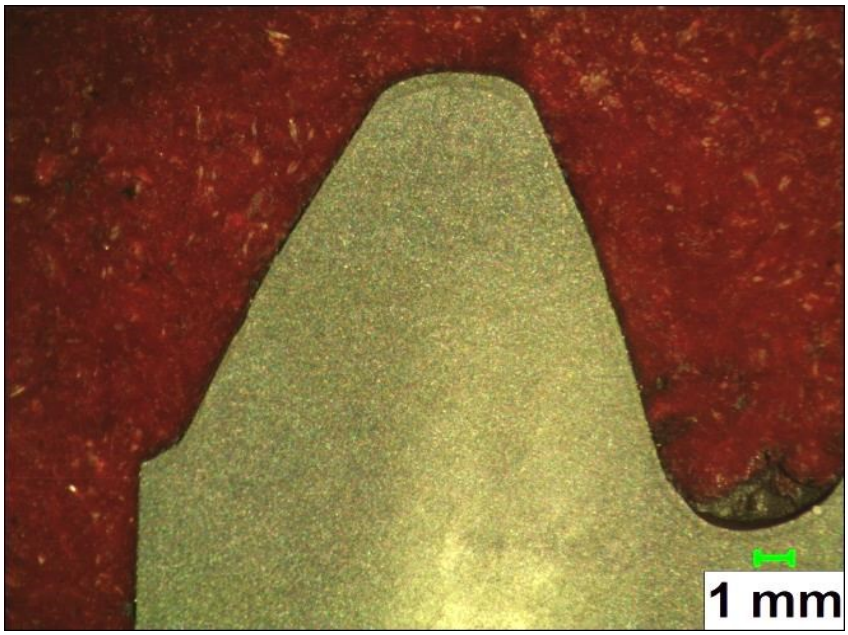

Figure 3.8 : Case depth observation for P = 3000 W, V_{sc} = 0.75 mm/s, w_r = 300 rpm and T_0 = 500 K

In the **Figure 3.10**it can be seen that the treatment was rather uniform at the top, the bottom and on the slope of the tooth, with only a slightly deeper case depth at the top. However, in this case, the case depth is very shallow (no more than 200-300 µm) and might not be sufficient to significantly improve material properties such as wear resistance. By comparison, gears treated by induction show much greater case depths on their teeth. However, the drawback of the induction process is that it requires very high power (tens of kilowatts) to perform a decent heat treatment.[39]

In **Figure 3.9**, the scanning velocity was decreased and, as expected, the treated zone is shallower than that shown in **Figure 3.8**. Indeed, a slower scanning velocity means that there will be more energy brought into the part. Thus, the case depth increases when the scanning velocity decreases. However the case depth is still greater at the top of the tooth than it is on the slope and at the bottom. In addition, it can be seen in **Figure 3.9** than the shape of the tooth was slightly bowed, due to the fact that the teeth originally had sharp corners that concentrated the heat. The simulation also demonstrated this, as can be seen in

Figure 3.3 where the temperature is higher in the sharp corners at the top of the tooth. This slight deformation is tolerable though considering the dimensions of the teeth.

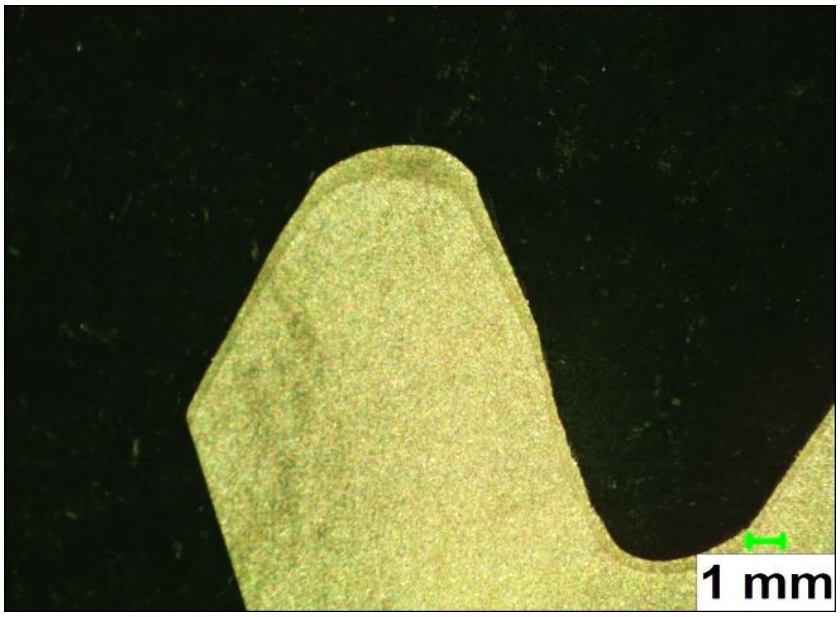

Figure 3.9 : Case depth observation for P = 3000 W, V_{sc}= 0.50 mm/s and w_r = 300 rpm and T_0 = 500 K

The simulation showed that the depth of the treatment largely depends on the preheating treatment. The closer the preheating temperature comes to the austenitization temperature, the deeper more the treated zone.

Figure 3.10 shows that all the teeth of the gears are roughly treated the same way with the same case depth observed on consecutive teeth.

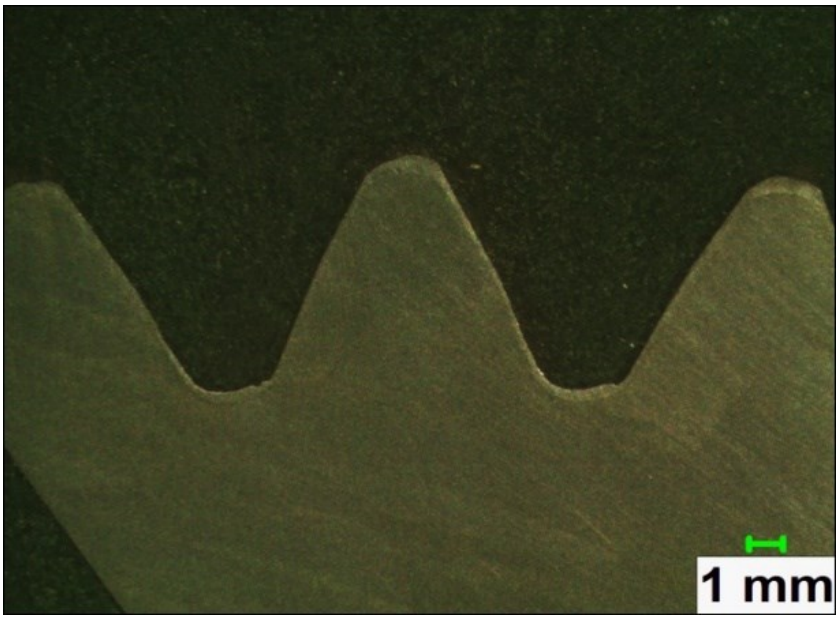

Figure 3.10 : Case depth observation for P = 2500 W, V_{sc} = 1 mm/s and w_r = 240 rpm and T_0 = 600 K

3.2.5.5-Comparison between simulation and experiment

Three tests are conducted to study the effect of the power and the rotation velocity on the case depth, as well as to validate the simulated hardness profile (see **Table 3.2**).

The scanning velocity and the preheating temperature, T_0, remain the same (0.75 mm/s and 600 K, respectively) for each of the three tests.

Figure 3.11, 3.12 and 3.13 show the hardness profiles obtained by both the simulation and the experiment according to the values presented in **Table 3.2**. In both the simulation and the experiment, the hardness profile is measured on the head of a tooth at its center.

Table 3.2 : Experimental matrix

Test	Power (W)	Rotation Speed (rpm)
1	2500	240
2	2500	300
3	3000	300

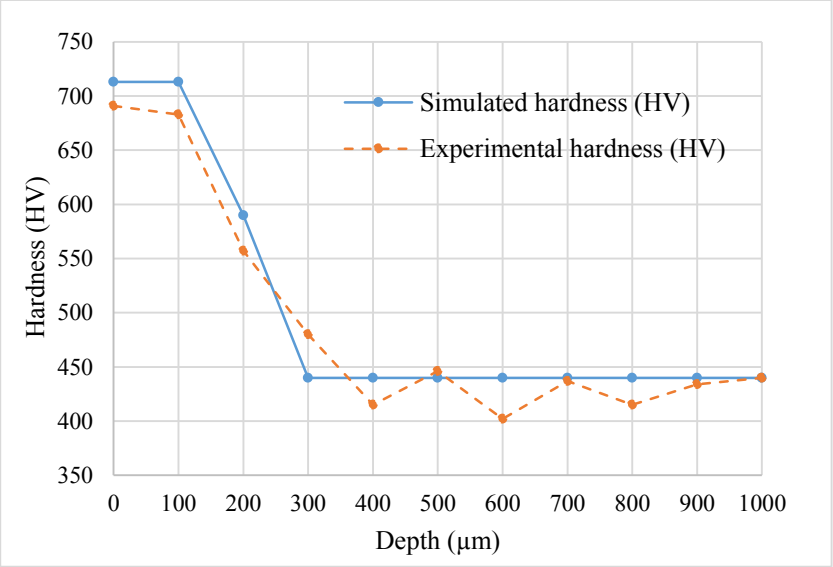

Figure 3.11 : Hardness curve for P = 2500 W, V_{sc} = 0.75 mm/s and w_r = 240 rpm and T_0 = 600 K

The figures clearly show three distinct zones: the treated zone, with a high hardness and a complete transformation into martensite; the transition zone, with a decreasing hardness where a partial transformation occurred; and the unaffected zone, where the hardness did not change. No transformation happened in the unaffected zone as the temperature did not reach the austenitization temperature.

The figures also show that the simulated hardness profile fairly closely follows the experimental hardness profile in each case. This means that with the adjusted 3D model, it is possible to predict the hardness profile for a given set of process parameters without conducting actual experiments, which could prove economically advantageous.

As expected, and as predicted by the simulation, **Figure 3.12** shows that the case depth decreases as the rotation speed increases (from 0.3-0.4 µm at 240 rpm to 0.2 µm at 300 rpm).

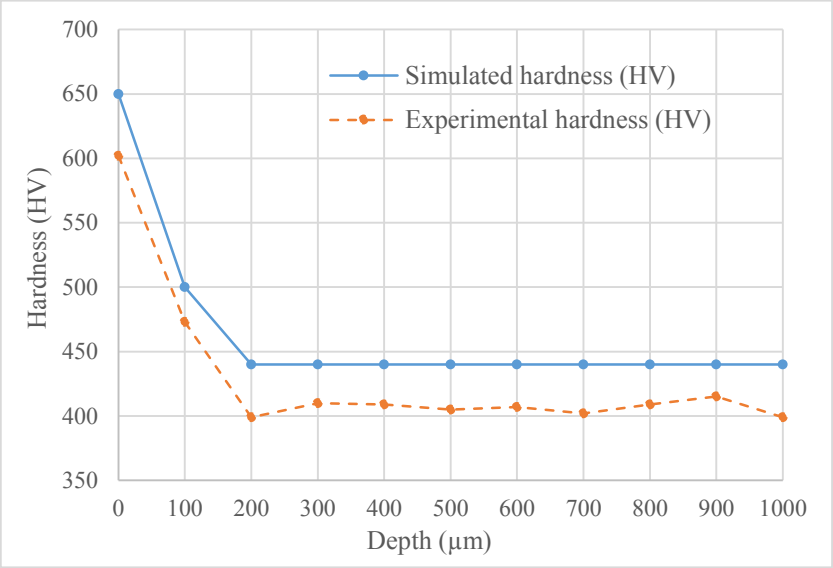

Figure 3.12 : Hardness curves for P = 2500 W, V_{sc} = 0.75 mm/s and w_r = 300 rpm and T_0 = 600 K

Figure 3.13 shows that the case depth increases as the power increases (from 0.2 µm with 2500 W to 0.3 µm with 3000 W).

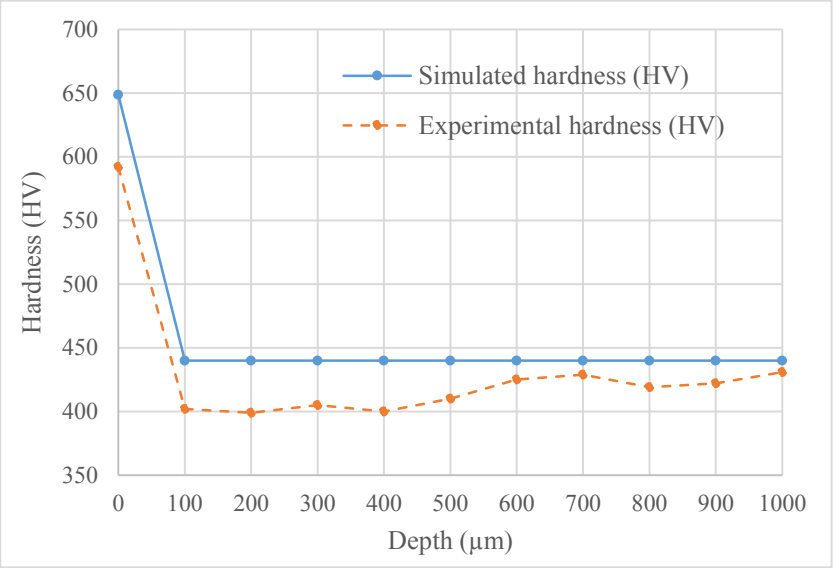

Figure 3.13 : Hardness curves for P = 3000 W, V_{sc} = 0.75 mm/s and w_r = 300 rpm and T_0 = 600 K

Table 3.3 shows the maximum absolute error and relative error, for each of the three tests, between the simulated hardness and the experimental harness. Because the reflection coefficient of the surface is hard to accurately estimate and has an effect on the case depth, there are some small differences between the simulated hardness profile and the experimental hardness profile. Indeed, a greater reflection coefficient, for example, means that less energy will be absorbed by the part. In this study, the reflection coefficient was assumed to be 0.6 (which is a common reflection coefficient for mild steels [3]), but it might be slightly different. In any case, using a surface coating could be a way to obtain a better estimation of the reflection coefficient.

Table 3.3 : Maximum absolute and relative hardness errors

Test	Absolute error (HV)	Relative error (%)
1	40	9.45
2	48	10.28
3	57	10

The maximum relative error for the three tests was 10.28 %, which indicates a decent model accuracy.

In the three previous tests, the hardness profile was measured on the top of a tooth. Indeed, as is shown in **Figure 3.9** and **Figure 3.10**, the base of the teeth is always less treated than the top. It appears than the chosen parameters for the three tests did not permit the formation of a significant case depth at the base of the gear teeth.

Moreover, the low rotation speeds (240 rpm or 300 rpm) induced a partial bowing of the tops of the teeth, as was shown in **Figure 3.9** and **Figure 3.10**. Increasing the rotation speed or decreasing the power or the scanning velocity to avoid bowing is useless, as this would result in no treatment at all.

In the next experiment, the power used during the preheating step is increased in order to reach a preheating temperature, T_0, of 873 K (the austenitization temperature Ac_1 being at 1000 K). The simulation showed that a greater preheating temperature allowed treatment at greater rotation speeds and lower power, and without the surface reaching the melting temperature.

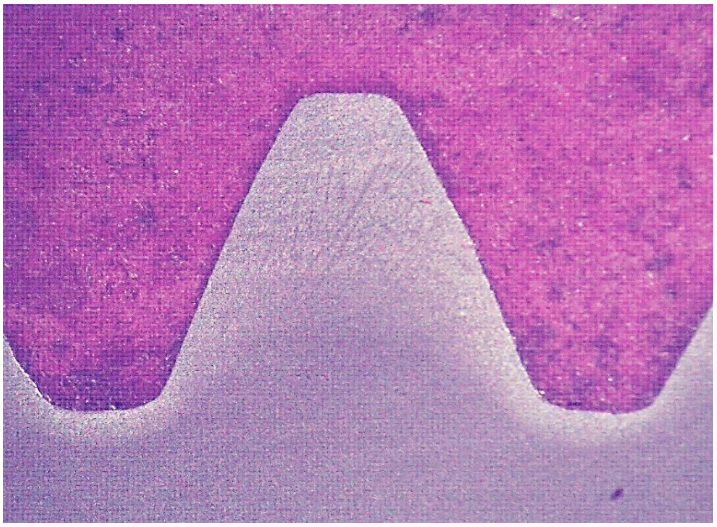

Figure 3.14 : Case depth observation for P= 1500W, V_{sc} = 0.75 mm/s and w_r = 750 rpm and T_0 = 873 K

Figure 3.14 shows a treatment with a power of 1500 W, a rotation speed of 750 rpm, a scanning velocity of 0.75 mm/s and a preheating temperature, T_0, of 873 K.

The figure clearly shows that there is treatment at the base of the teeth.

The case depth obtained is very comparable to the case depth obtained by the induction process [39] but is achieved using a much lower input power (only 1500 W was used in this study, compared to the tens of thousands of watts usually required to treat gear teeth by induction). It is also noteworthy that **Figure 3.14** shows that the top of the tooth is not bowed as the melting temperature was not reached for this test. This is especially apparent in comparing **Figure 3.9** and **Figure 3.14**.

The case depth achieved at the top of the gear with a high preheating temperature is much deeper than that seen using a low preheating temperature.

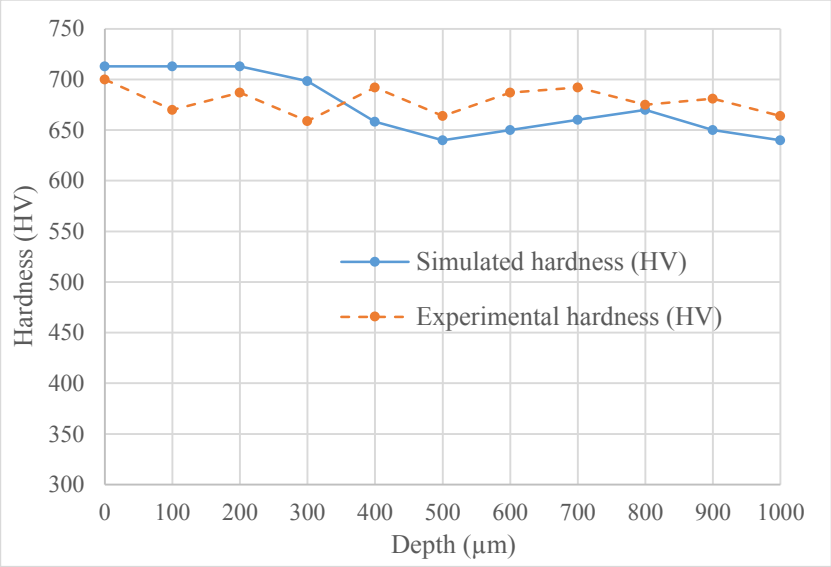

Figure 3.15 : Hardness curves for P= 1500 W, V_{sc} = 0.75 mm/s and w_r = 750 rpm and T_0 = 873 K at the top of the tooth

Figure 3.15 and **Figure 3.16** show the simulated and the predicted hardness in the case of a preheating temperature of T_0 = 873 K. The case depth at the top of the teeth exceeds 1 mm, while the case depth at the base of the teeth is about 0.2-0.3 mm. Once again, it appears that the base of the gear teeth is difficult to properly treat compared to the top.

Once again, the simulation was able to fairly closely match the experiment, as it is shown by **Table 3.4**, which gives the maximum absolute and relative errors for the top and the bottom of the gear teeth.

Table 3.4 **:** Comparison between simulation and experiment for T_0 = 873 K

Location	Absolute error (HV)	Relative error (%)
Top of the tooth	43	6.41
Foot of the tooth	40	8.33

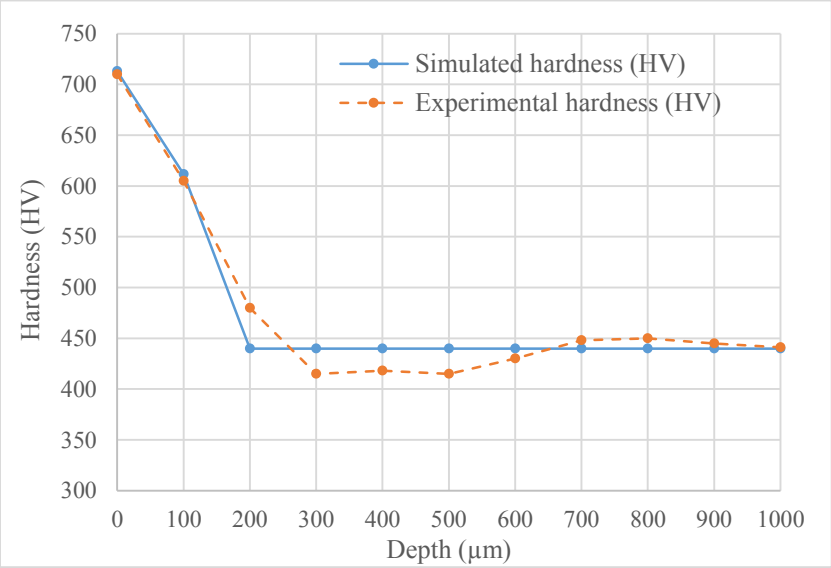

Figure 3.16 : Hardness curves for P = 1500W, V_{sc} = 0.75 mm/s and w_r = 750 rpm and T_0 = 873 K at the foot of the tooth

3.2.6-Conclusion

The Thermal analysis of surface transformation hardening of gears using laser is conducted using a 3D numerical model validated by an experimental procedure. A 3D model of the laser hardening process in the case of gear teeth is implemented on a commercial software capable of solving the governing heat flow equation using the finite element method. By extracting the temperature data, it is possible to produce a simulated hardness profile using the Ashby and Easterling equations. The simulation proves to be quite accurate with a maximum relative error around 10 %. The observations made with the

simulation are easily verified by the experiment. The case depth increases as the power increases and/or as the rotation speed decreases. However, due to the geometry of the gear teeth, low rotation speeds with high laser power generate partial melting of the tips of the teeth. The simulation also shows that the preheating temperature plays a major role in the quality of the treatment. Indeed, with a higher preheating temperature, it is possible to obtain a very decent case depth at both the top and the base of the teeth. This is validated by the experiment where a case depth comparable with what can be obtained by induction is produced. From the results obtained in this study, it appears that it would be possible to develop an industrial process to treat gear teeth by laser using relatively low power and rotation speeds. Optimizing the preheating process used in this study in order to reach a good preheating temperature seems to be a solution. An interesting investigation would be to test the ultimate bending strength as well as the wear resistance of gear teeth that have been properly treated by laser.

3.2.7-Acknowledgment

The authors would like to thank AlKhader Borki, research assistant at the University of Québec at Rimouski, for his involvement in the experimental setup and procedure

CONCLUSION GÉNÉRALE

Cette étude a montré qu'il est possible actuellement de modéliser numériquement et avec une bonne précision le procédé de traitement thermique superficiel au laser des matériaux à l'aide d'un logiciel de calculs par la méthode des éléments finis. Bien que la modélisation soit longue à mettre en œuvre à cause du nombre important de paramètres, le modèle s'avère étonnamment précis et robuste démontrant une concordance remarquable entre les prédictions et les mesures expérimentales.

Dès lors, une prédiction numérique du résultat en fonction des paramètres d'entrée devient envisageable et permet d'éviter le long et coûteux processus essai-erreur. La première phase du projet a permis d'établir un premier modèle numérique fonctionnel du procédé dans le cas simple d'un parallélépipède rectangle avec une source de chaleur en translation. Dans cette étude, un logiciel de calculs par élément fini fut utilisé pour résoudre l'équation de propagation de la chaleur dans le matériau avec des paramètres dépendant de la température. L'historique de température fut ensuite extrait pour établir les profils de dureté — dureté en fonction de la profondeur — grâce aux équations métallurgiques. La vérification expérimentale a donné de bons résultats avec des profils de dureté prédits très proches des profils de dureté réels mesurés par micro-indentation sous les mêmes paramètres de contrôle. Cependant, il est vite apparu que la modélisation par une source de chaleur compliquait la mise en place du modèle (notamment par la difficulté à déterminer le coefficient d'extinction A_c) ainsi que la résolution de ce dernier. De plus, le modèle serait difficilement adaptable à des géométries plus complexes.

C'est la raison pour laquelle il a été décidé de changer le mode dans le deuxième chapitre et de modéliser le laser par un flux de chaleur à travers la surface du matériau au lieu d'une source de chaleur. Cette modélisation nous a permis d'éviter le coefficient d'extinction problématique ainsi que de préparer le passage aux géométries plus complexes par une approche plus robuste. Dans ce deuxième chapitre, la géométrie utilisée est la même que pour le premier chapitre avec le même mouvement de translation. Toutefois, quelques tests ont été nécessaires afin d'ajuster le coefficient de réflexion de matériau qui semblait dépendant de la température en surface et donc des paramètres de contrôle.

Comme dans le premier chapitre, les résultats expérimentaux ont vite montré une concordance avec les résultats donnés par la simulation. Cependant, la modélisation par flux de chaleur a permis de diminuer drastiquement le temps de calcul et donc de générer un grand nombre de données. Le grand nombre de données a permis de générer des formules de régression très précises reliant la profondeur et la largeur durcie aux paramètres de contrôle du procédé. Le réseau de neurones artificiels, une fois entrainé, pouvait fonctionner indépendamment de tous logiciels de calculs par éléments finis et donnait des résultats très proches de la réalité pourvu que les paramètres d'entrées fussent inclus dans sa plage d'entrainement. Un tel réseau de neurones artificiels pourrait éventuellement servir à l'élaboration de logiciels avec des applications industrielles dans le domaine du traitement thermique au laser.

Ce modèle par flux de chaleur a permis un passage relativement facile aux géométries complexes dans le troisième chapitre. Dans ce troisième chapitre, un mouvement de rotation a été rajouté en plus du mouvement de translation. Le modèle a permis de simuler le traitement au laser complet des dents d'un engrenage monté sur un tour. Pour traiter convenablement les dents d'un engrenage sans causer de déformations thermiques, il est apparu qu'un préchauffage à basse puissance avec un balayage en va-et-vient est nécessaire afin d'approcher la température des dents le plus près possible de la température d'austénitisation. Le traitement lui-même consiste ensuite en un seul balayage à forte puissance. Les résultats expérimentaux ont démontré que les résultats donnés par la simulation étaient proches de la réalité avec des profils de dureté simulés et réels presque identique. La simulation a aussi montré que, par ce procédé, le sommet de la dent est toujours traité plus en profondeur que le pied. Cette observation a ensuite été confirmée plus tard par les essais expérimentaux. En revanche, à cause de la géométrie complexe et du mouvement de rotation, le temps de simulation a drastiquement augmenté par rapport à celui observé dans le deuxième chapitre. Il est toujours possible de générer un grand nombre de données et de les utiliser pour réaliser des études statistiques ou entrainer un réseau de neurones artificiels capable de prédire les profondeurs et largeurs traitées pour des paramètres d'entrées donnés, mais le procédé est significativement plus long. Par

ailleurs, le banc d'essai fabriqué pour la validation expérimentale a permis d'établir un procédé de traitement des dents d'engrenages par laser donnant des résultats relativement identiques à ceux obtenus par le traitement par induction. Ce procédé requiert des niveaux puissances très inférieurs à ceux mis en jeu dans le procédé par induction. Il a aussi l'avantage d'être adaptable à n'importe quel diamètre d'engrenage contrairement au procédé par induction qui requiert un équipement spécifique pour chaque diamètre d'engrenage.

D'une façon générale, les modèles développés ont permis de prédire assez convenablement les résultats d'un traitement thermique superficiel au laser, pour des ensembles de paramètres de contrôle donnés, sans recourir à la coûteuse méthode consistant à avancer par échecs/corrections avec des essais expérimentaux. Une piste intéressante serait d'utiliser ces modèles afin de générer un grand nombre de données pour entrainer des réseaux de neurones bien plus perfectionnés que celui du deuxième chapitre. Ces réseaux de neurones pourraient servir à créer des logiciels que les industriels utiliseraient pour économiser en temps et en coût. Aussi, le procédé de traitement au laser d'un engrenage monté sur un tour développé dans le troisième chapitre pourrait avoir de possibles applications industrielles s'il était davantage approfondi.

RÉFÉRENCES BIBLIOGRAPHIQUES

[1] Ion JC. Laser processing of engineering materials : principles, procedure and industrial application. Amsterdam: Elsevier/Butterworth-Heinemann; 2005.
[2] Kannatey-Asibu E. Principles of laser materials processing. Hoboken, N.J.: Wiley; 2009.
[3] Steen WM, Mazumber J. Laser Material Processing. 4th ed. ed. London: Springer; 2010.
[4] Chipman J. Thermodynamics and phase diagram of the Fe-C system. MT. 1972;3:55-64.
[5] Ashby MF, Easterling KE. The transformation hardening of steel surfaces by laser beams—I. Hypo-eutectoid steels. Acta Metallurgica. 1984;32:1935-48.
[6] Krauss G. Steels : heat treatment and processing principles. Materials Park, Ohio: ASM International; 1993.
[7] Paul E. Materials and Processes in Manufacturing (8th edition): Macmillan; 1997.
[8] Shiue RK, Chen C. Laser transformation hardening of tempered 4340 steel. MTA. 1992;23:163-70.
[9] Zhang H, Shi Y, Xu C, Kutsuna M. Comparison of contact fatigue strength of carbon case hardening and laser hardening of gears. Surface engineering. 2004;20:117-20.
[10] America LIo, Ready JF, Farson DF. LIA handbook of laser materials processing. 1st ed. ed. Orlando, Fla. : Magnolia Publishing: Laser Institute of America; 2001.
[11] Totten GE. Handbook of residual stress and deformation of steel: ASM international; 2002.
[12] Steen WM. Laser Material Processing. 4th ed.. ed. London: Springer; 2010.
[13] Davis M, Kapadia P, Dowden J, Steen WM, Courtney CHG. Heat hardening of metal surfaces with a scanning laser beam. Journal of Physics D: Applied Physics. 1986;19:1981.
[14] Mioković T, Schulze V, Vöhringer O, Löhe D. Prediction of phase transformations during laser surface hardening of AISI 4140 including the effects of inhomogeneous austenite formation. Materials Science and Engineering: A. 2006;435–436:547-55.
[15] Skvarenina S, Shin YC. Predictive modeling and experimental results for laser hardening of AISI 1536 steel with complex geometric features by a high power diode laser. Surface and Coatings Technology. 2006;201:2256-69.
[16] Tobar MJ, Álvarez C, Amado JM, Ramil A, Saavedra E, Yáñez A. Laser transformation hardening of a tool steel: Simulation-based parameter optimization and experimental results. Surface and Coatings Technology. 2006;200:6362-7.
[17] Patwa R, Shin YC. Predictive modeling of laser hardening of AISI5150H steels. International Journal of Machine Tools and Manufacture. 2007;47:307-20.

[18] Orazi L, Fortunato A, Cuccolini G, Tani G. An efficient model for laser surface hardening of hypo-eutectoid steels. Applied Surface Science. 2010;256:1913-9.
[19] Antony J, Jiju Antony F. Teaching the Taguchi method to industrial engineers. Work Study. 2001;50:141-9.
[20] Badkar D, Pandey K, Buvanashekaran G. Parameter optimization of laser transformation hardening by using Taguchi method and utility concept. Int J Adv Manuf Technol. 2011;52:1067-77.
[21] Doane D. Application of hardenability concepts in heat treatment of steel. Journal of Heat Treating. 1979;1:5-30.
[22] Yang ST, Matthews MJ, Elhadj S, Cooke D, Guss GM, Draggoo VG, et al. Comparing the use of mid-infrared versus far-infrared lasers for mitigating damage growth on fused silica. Appl Opt. 2010;49:2606-16.
[23] McDaniels RL, White SA, Liaw K, Chen L, McCay MH, Liaw PK. Effects of a laser surface processing induced heat-affected zone on the fatigue behavior of AISI 4340 steel. Materials Science and Engineering: A. 2008;485:500-7.
[24] Chen SL, Shen D. Optimisation and Quantitative Evaluation of the Qualities for Nd-YAG Laser Transformation Hardening. Int J Adv Manuf Technol. 1999;15:70-8.
[25] Benyounis KY, Olabi AG, Hashmi MSJ. Effect of laser welding parameters on the heat input and weld-bead profile. Journal of Materials Processing Technology. 2005;164–165:978-85.
[26] Sathiya P, Abdul Jaleel MY, Katherasan D. Optimization of welding parameters for laser bead-on-plate welding using Taguchi method. Prod Eng Res Devel. 2010;4:465-76.
[27] Hagan MT, Demuth HB, Beale MH. Neural network design: Pws Boston; 1996.
[28] Ciurana J, Arias G, Ozel T. Neural Network Modeling and Particle Swarm Optimization (PSO) of Process Parameters in Pulsed Laser Micromachining of Hardened AISI H13 Steel. Materials & Manufacturing Processes. 2009;24:358-68.
[29] Pan QY, Huang WD, Song RG, Zhou YH, Zhang GL. The improvement of localized corrosion resistance in sensitized stainless steel by laser surface remelting. Surface and Coatings Technology. 1998;102:245-55.
[30] Munteanu A. SURFACE HARDNESS PREDICTION USING ARTIFICIAL NEURAL NETWORKS IN CASE OF ELECTRON BEAM MACHNING PROCESS. 2012.
[31] Haykin S. Neural networks: a comprehensive foundation, 1994. Mc Millan, New Jersey. 2010.
[32] Principe J, Euliano N, Lefebvre W. Neural and adaptive systems: fundamentals through simulations. 2000. John Wiley and Sons, New York, pgs.119:514.
[33] Munikamal T, Sundarraj S. Modeling the Case Hardening of Automotive Components. Metall and Materi Trans B. 2013;44:436-46.
[34] Steen W, Courtney C. Surface heat treatment of EnS steel using a 2kW continuous-wave CO2 laser. Metals Technology. 1979;6:456-62.
[35] Kou S, Sun DK, Le YP. A Fundamental Study of Laser Transformation Hardening. MTA. 1983;14:643-53.
[36] Komanduri R, Hou Z. Thermal analysis of the laser surface transformation hardening process. International Journal of heat and mass transfer. 2001;44:2845-62.

[37] Komanduri R, Hou Z. Thermal analysis of laser surface transformation hardening—optimization of process parameters. International Journal of Machine Tools and Manufacture. 2004;44:991-1008.
[38] Billaud G, El Ouafi A, Barka N. ANN Based Model for Estimation of Transformation Hardening of AISI 4340 Steel Plate Heat-Treated by Laser. Materials Sciences and Applications. 2015;6:978.
[39] Barka N, Chebak A, El Ouafi A, Jahazi M, Menou A. A New Approach in Optimizing the Induction Heating Process Using Flux Concentrators: Application to 4340 Steel Spur Gear. J of Materi Eng and Perform. 2014;23:3092-9.